

# **Synthesis and Photophysical Properties of the First Au(III)-Ag(I) Aggregates.**

Julio Fernandez-Cestau,\* Raquel J. Rama, Luca Rocchigiani, Benoit Bertrand, Elena Lalinde, Mikko Linnolahti, and Manfred Bochmann

## **SUPPORTING INFORMATION**

|           |                                       |
|-----------|---------------------------------------|
| <b>S1</b> | <b>Synthesis and Characterization</b> |
| <b>S2</b> | <b>X-ray Crystallography</b>          |
| <b>S3</b> | <b>Photophysical Properties</b>       |
| <b>S4</b> | <b>Theoretical Calculations</b>       |
| <b>S5</b> | <b>Diffusion NMR</b>                  |
| <b>S6</b> | <b>References</b>                     |

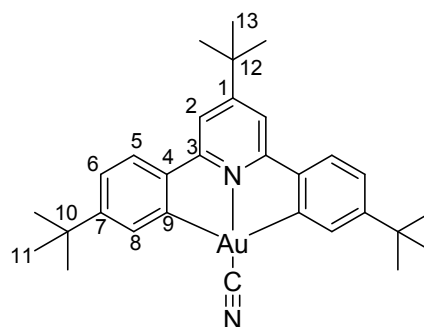
## S1. Synthesis and Characterization

When required, manipulations were performed using standard Schlenk techniques under dry nitrogen or using an M. Braun glove box. Nitrogen was purified by passing through columns of supported  $P_2O_5$  with moisture indicator, and of activated 4 Å molecular sieves. Anhydrous solvents were freshly distilled from appropriate drying agents. Infrared spectra were recorded using a Perkin Elmer Spectrum 65 FT-IR spectrometer with a diamond ATR attachment. Elemental analyses were carried out at London Metropolitan University.  $^1H$ ,  $^{13}C\{^1H\}$  and  $^{19}F$  spectra were recorded using a Bruker Avance DPX-300 spectrometer.  $CD_2Cl_2$  was stored on 4 Å molecular sieves prior to use.  $^1H$  NMR spectra (300.13 MHz) were referenced to the residual protons of the deuterated solvent used.  $^{13}C\{^1H\}$  NMR spectra (75.47 MHz) were referenced internally to the D-coupled  $^{13}C$  resonances of the NMR solvent.  $^{19}F\{^1H\}$  NMR spectra (282.38 MHz) were referenced to  $CFC l_3$ .

$(C^{\wedge}N^{tBu^{\wedge}}C)AuCN$  [ **$tBu$ -pyAuCN**] was synthesized (90 % yield) by modifying a reported procedure (Fernandez-Cestau, J. et al., *Chem. Commun.* **2015**, 51, 16629-16632.).

Anal. Calcd for  $C_{30}H_{35}N_2Au$  (620.6): C, 58.06; H, 5.68; N, 4.51. Found: C, 57.87; H, 5.85; N, 4.48.  $^1H$  NMR ( $CD_2Cl_2$ , 300.13 MHz, 25°C):  $\delta$  8.02 (d,  $^4J_{H-H} = 1.7$  Hz, 2 H,  $H^8$ ), 7.58 (d,  $^3J_{H-H} = 8.2$  Hz, 2 H,  $H^5$ ), 7.43 (s, 2 H,  $H^2$ ), 7.34

(dd,  $^3J_{H-H} = 8.2$  Hz,  $^4J_{H-H} = 1.8$  Hz, 2 H,  $H^6$ ), 1.42 (s, 9 H,  $tBu_{py}$ ), 1.37 (s, 18 H,  $tBu$ ).  $^{13}C\{^1H\}$  NMR ( $CD_2Cl_2$ , 75.48 MHz):  $\delta$  168.7 ( $C^1$ ), 166.1 ( $C^9$ ), 165.6 ( $C^{3/4}$ ), 164.8 ( $C^9$ ), 156.0 ( $C^{3/4}$ ), 146.20 ( $C^7$ ), 134.1 ( $C^8$ ), 124.9 ( $C^5$ ), 124.2 ( $C^6$ ), 114.0 ( $C^2$ ), 36.2 ( $C^{12}$ ), 35.3 ( $C^{10}$ ), 30.9 ( $C^{11}$ ), 30.0 ( $C^{13}$ ), CN not detected. [ **$tBu$ -pyAu $^{13}C$ N**]  $^{13}C\{^1H\}$  NMR ( $CD_2Cl_2$ , 75.48 MHz): Similar to [ **$tBu$ -pyAuCN**] but with the signal that corresponds to the cyanide group as a singlet at 115.9 ppm.



### $[{(C^{\wedge}N^{pz^{\wedge}}C)Au(CN))_2Ag](SbF_6) 1SbF_6$

$(C^{\wedge}N^{pz^{\wedge}}C)AuCN$  (22.6 mg, 0.04 mmol) was dissolved in  $CH_2Cl_2$  (ca. 5 mL) and loaded in one side of a double crystallization tube (See Figure S1).  $AgSbF_6$  (13.8 mg, 0.04 mmol) in THF was loaded into the other chamber of this tube. Both solutions were layered with THF and the whole volume of the tube was filled with THF. Slow diffusion generated orange crystals. One crystal was selected for X-Ray diffraction studies but the low quality of the

crystal only allowed to report the connectivity. The rest of the material was filtered off, washed with THF and air dried (26.4 mg, 0.018 mmol, 89 % yield). Anal. Calcd for  $C_{50}H_{52}AgAu_2F_6N_6Sb$  (1474.6): C, 40.73; H, 3.55; N, 5.70. Found: C, 40.92; H, 3.59; N, 5.63. IR ( $cm^{-1}$ ):  $\nu(C \equiv N)$  2218 (w). The low solubility of the complex precludes the characterization by NMR spectroscopy.

**$[\{(C^{\wedge}N^{pz^{\wedge}}C)Au(CN)\}_2Ag](ClO_4) 1ClO_4$**

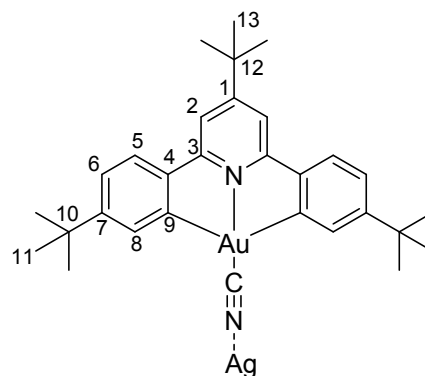
The complex was made from  $(C^{\wedge}N^{pz^{\wedge}}C)AuCN$  (22.6 mg, 0.04 mmol) and  $AgClO_4$  (2.2 mg, 0.04 mmol) following the method described for **1SbF<sub>6</sub>** as an orange microcrystalline solid (21.4 mg, 0.016 mmol, 80 % yield). Anal. Calcd for  $C_{50}H_{52}AgAu_2ClN_6O_4$  (1338.3): C, 44.88; H, 3.92; N, 6.28. Found: C, 45.01; H, 4.10; N, 6.27. IR ( $cm^{-1}$ ):  $\nu(C \equiv N)$  2209 (w); 2197 (sh); 2187 (sh). The low solubility of the complex precluded characterization by NMR spectroscopy.



**Figure S1.1:** Experimental setup for the direct synthesis of complex  $[\{(C^{\wedge}N^{pz^{\wedge}}C)Au(CN)\}_2Ag](SbF_6) 1SbF_6$

**$[\{(C^{\wedge}N^{tBu^{\wedge}}C)Au(CN)\}_2Ag](SbF_6)_2$**

Under nitrogen, a  $CH_2Cl_2$  solution (10 mL) of  $(C^{\wedge}N^{tBu^{\wedge}}C)AuCN$  (24.8 mg, 0.04 mmol) was treated with  $AgSbF_6$  (27.6 mg, 0.08 mmol). A color change from pale yellow to deeper yellow was noted. The solution was filtered through Celite and the solvent was evaporated. The yellow residue was precipitated with light petroleum, filtered off and dried in air to give the pure product as a yellow powder. (30.1 mg, 0.019 mmol, 95 % yield). Anal.



Calcd for  $C_{60}H_{70}AgAu_2F_6N_4Sb$  (1584.8): C, 45.47; H, 4.45; N, 3.54. Found: C, 45.55; H, 4.25; N, 3.53. IR ( $cm^{-1}$ ):  $\nu(C \equiv N)$  2196 (w); 2180 (w); 2165 (sh).  $^1H$  NMR ( $CD_2Cl_2$ , 300.13 MHz, 25°C):  $\delta$  7.93 (d,  $^4J_{H-H} = 1.9$  Hz, 2 H, H<sup>8</sup>), 7.62 (d,  $^3J_{H-H} = 8.2$  Hz, 2 H, H<sup>5</sup>), 7.47 (s, 2 H, H<sup>2</sup>), 7.40 (dd,  $^3J_{H-H} = 8.2$  Hz,  $^4J_{H-H} = 1.9$  Hz, 2 H, H<sup>6</sup>), 1.44 (s, 9 H,  $tBu_{py}$ ), 1.39 (s, 18 H,  $tBu$ ).  $^{13}C\{^1H\}$  NMR ( $CD_2Cl_2$ , 75.48 MHz):  $\delta$  170.1 ( $C^1$ ), 166.4 ( $C^9$ ), 166.3 ( $C^{3/4}$ ), 156.9 ( $C^{3/4}$ ), 146.5 ( $C^7$ ), 134.1 ( $C^8$ ), 125.9 ( $C^5$ ), 125.2 ( $C^6$ ), 114.9 ( $C^2$ ), 36.7 ( $C^{12}$ ), 36.8 ( $C^{10}$ ), 31.3 ( $C^{11}$ ), 30.4 ( $C^{13}$ ), CN not observed.

**$[\{(C^{\wedge}N^{tBu^{\wedge}}C)Au(^{13}CN)\}_2Ag](SbF_6)_2$**   $^{13}C$  This complex was prepared similarly but starting from  $(C^{\wedge}N^{tBu^{\wedge}}C)Au(^{13}CN)$  (5.0 mg, 0.008 mmol) and  $AgSbF_6$  (5.5 mg, 0.016 mmol).  $^{13}C\{^1H\}$  NMR ( $CD_2Cl_2$ , 75.48 MHz): The CN signal was observed at 124.3 ppm.

**$[\{(C^{\wedge}N^{tBu^{\wedge}}C)Au(CN)\}_2Ag](ClO_4)_2$**

The complex was made from  $(C^{\wedge}N^{tBu^{\wedge}}C)Au(CN)$  (25.0 mg, 0.04 mmol) and  $AgClO_4$  (16.6 mg, 0.08 mmol) following the same method as for **2SbF<sub>6</sub>** and isolated as a pale yellow solid (27.5 mg, 0.019 mmol, 95 % yield). Anal. Calcd for  $C_{60}H_{70}AgAu_2ClN_4O_4$  (1448.5): C, 49.75; H, 4.87; N, 3.87. Found: C, 49.70; H, 4.96; N, 3.50. IR ( $cm^{-1}$ ):  $\nu(C \equiv N)$  2195 (w); 2185 (w).  $^1H$  NMR ( $CD_2Cl_2$ , 300.13 MHz, 25°C):  $\delta$  7.95 (d,  $^4J_{H-H} = 1.5$  Hz, 2H, H<sup>8</sup>), 7.60 (d,  $^3J_{H-H} = 8.2$  Hz, 2H, H<sup>5</sup>), 7.46 (s, 2H, H<sup>2</sup>), 7.39 (dd,  $^3J_{H-H} = 8.2$ ,  $^4J_{H-H} = 1.5$  Hz, 1H), 1.44 (s, 9 H,  $tBu_{py}$ ), 1.39 (s, 18 H,  $tBu$ ).  $^{13}C\{^1H\}$  NMR ( $CD_2Cl_2$ , 75.48 MHz):  $\delta$  170.0 ( $C^1$ ), 166.5 ( $C^9$ ), 165.3 ( $C^{3/4}$ ), 156.8 ( $C^{3/4}$ ), 146.4 ( $C^7$ ), 134.1 ( $C^8$ ), 125.8 ( $C^5$ ), 125.1 ( $C^6$ ), 124.0 (CN), 114.8 ( $C^2$ ), 36.7 ( $C^{12}$ ), 35.8 ( $C^{10}$ ), 31.3 ( $C^{11}$ ), 30.4 ( $C^{13}$ ).  **$[\{(C^{\wedge}N^{tBu^{\wedge}}C)Au(^{13}CN)\}_2Ag](ClO_4)_2$**   $^{13}C$ . This complex was prepared from  $(C^{\wedge}N^{tBu^{\wedge}}C)Au(^{13}CN)$  (5.0 mg, 0.008 mmol) and

AgClO<sub>4</sub> (3.3 mg, 0.016 mmol). <sup>13</sup>C{<sup>1</sup>H} NMR (CD<sub>2</sub>Cl<sub>2</sub>, 75.48 MHz): CN signal at 124.7 ppm.

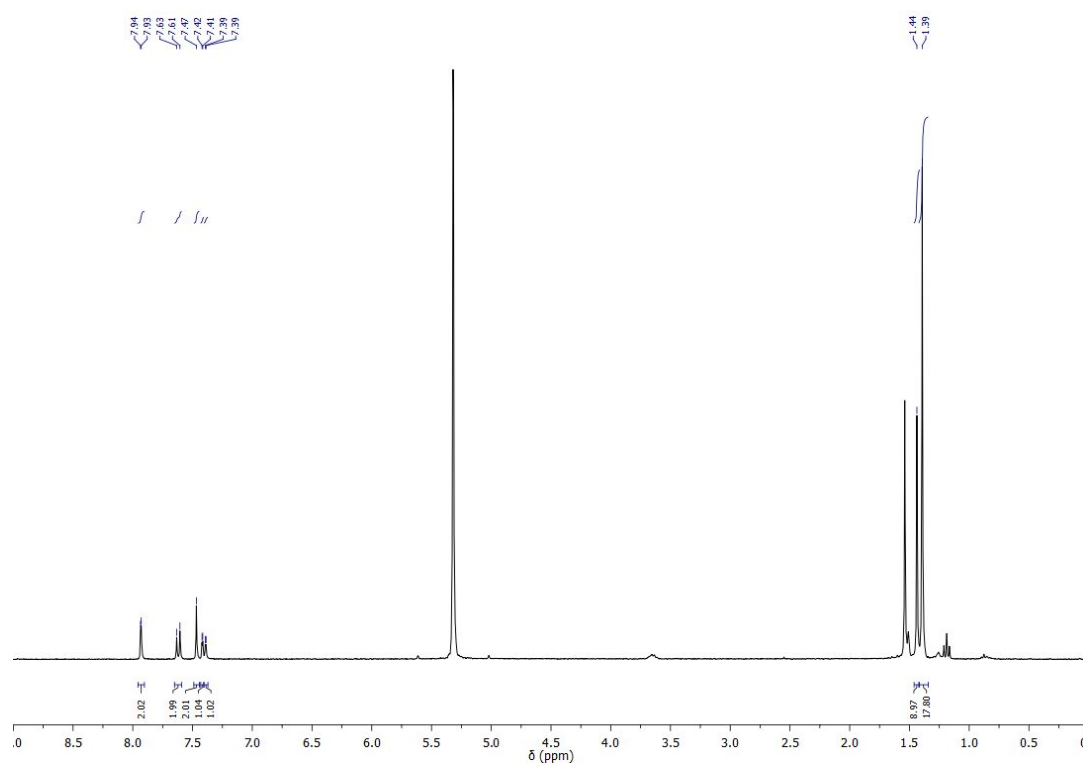


**Figure S1.2.** <sup>1</sup>H NMR spectrum at 25°C of **2SbF<sub>6</sub>**.

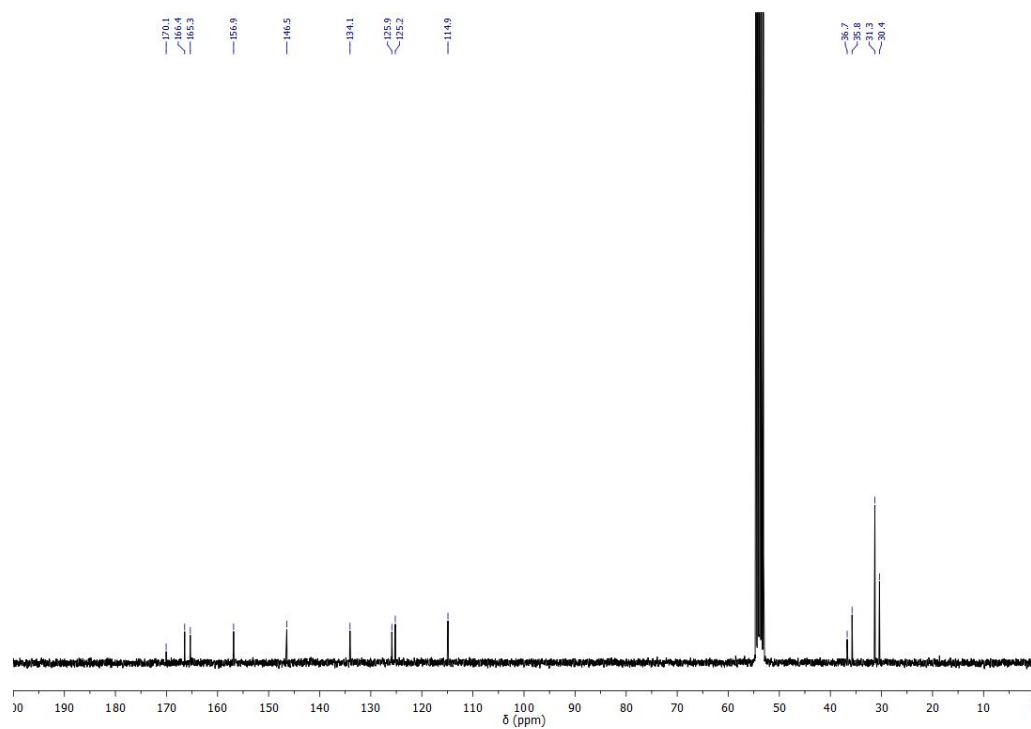
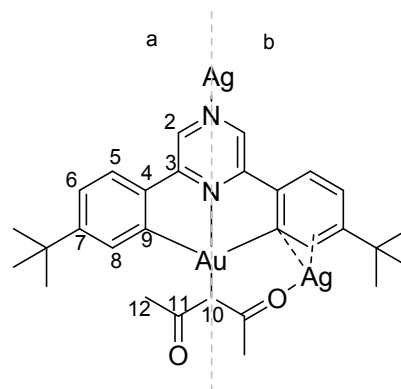


**Figure S1.3.** <sup>13</sup>C NMR spectrum at 25°C of **2SbF<sub>6</sub>**.

**[{((C<sup>Npz</sup>C)Au(acac))<sub>2</sub>Ag}<sub>2</sub>{Ag(SbF<sub>6</sub>)<sub>4</sub>}<sub>2</sub>] 3SbF<sub>6</sub>**

Under nitrogen, a CH<sub>2</sub>Cl<sub>2</sub> solution (c.a. 10 mL) of (C<sup>Npz</sup>C)Au(acac) (12.8 mg, 0.02 mmol) was treated with AgSbF<sub>6</sub> (14.0 mg, 0.04 mmol), causing a color change from yellow to orange. The solution was filtered through Celite and the solvent evaporated. The orange residue was precipitated with light petroleum, filtered off and dried in air to give the pure product as an orange powder (18.7 mg, 0.019 mmol, 95 % yield). Anal. Calcd for



C<sub>116</sub>H<sub>132</sub>N<sub>8</sub>Ag<sub>4</sub>Au<sub>4</sub>F<sub>24</sub>O<sub>8</sub>Sb<sub>4</sub> (3928,72): C, 35.46; H, 3.39; N, 2.85. Found: C, 35.55; H, 3.70; N, 2.87. IR (cm<sup>-1</sup>): ν(C=O) 1710 (*sh*), 1677 (*m*). <sup>1</sup>H NMR (CD<sub>2</sub>Cl<sub>2</sub>, 300.13 MHz, -40°C): δ 9.30 (*s*, 1H, H<sup>2a</sup>), 8.92 (*s*, 1H, H<sup>2b</sup>), 8.13 (*d*, <sup>3</sup>J<sub>H-H</sub> = 8.1 Hz, 1H, H<sup>5a</sup>), 7.61 (*d*, <sup>3</sup>J<sub>H-H</sub> = 8.1 Hz, 1H, H<sup>6a</sup>), 7.45 (*bs*, 2H, H<sup>8a,8b</sup>), 7.18 (*d*, <sup>3</sup>J<sub>H-H</sub> = 7.6 Hz, 1H, H<sup>5b</sup>), 7.04 (*d*, <sup>3</sup>J<sub>H-H</sub> = 7.6 Hz, 1H, H<sup>6b</sup>), 5.01 (*s*, 1H, H<sup>10</sup>), 2.54 (*s*, 3H, H<sup>12b</sup>), 2.06 (*s*, 3H, H<sup>12a</sup>), 1.37 (*s*, 9H, <sup>t</sup>Bu<sup>a</sup>), 0.80 (*s*, 9H, <sup>t</sup>Bu<sup>b</sup>). <sup>1</sup>H NMR (CD<sub>2</sub>Cl<sub>2</sub>, 300.13 MHz, 25°C): δ 9.18 (*s*, 2H, H<sup>2</sup>), 7.97-7.15 (*m*, 6H, H<sup>5,6,8</sup>), 4.99 (*s*, 1H, H<sup>10</sup>), 2.33 (*bs*, 6H, H<sup>12</sup>), 1.30-1.06 (*m*, 18H, <sup>t</sup>Bu). <sup>13</sup>C{<sup>1</sup>H} NMR the low solubility precludes its characterization by <sup>13</sup>C NMR.

**[{((C<sup>Npz</sup>C)Au(acac))<sub>2</sub>Ag}<sub>2</sub>{Ag(ClO<sub>4</sub>)<sub>4</sub>}<sub>2</sub>] 3ClO<sub>4</sub>**

The complex was made from (C<sup>Npz</sup>C)Au(acac)<sub>2</sub> (12.8 mg, 0.02 mmol) and AgClO<sub>4</sub> (8.2 mg, 0.04 mmol) following the method described for **3SbF<sub>6</sub>**. The complex was isolated as an orange powder (18.7 mg, 0.019 mmol, 95 % yield). Anal. Calcd for C<sub>116</sub>H<sub>132</sub>Ag<sub>4</sub>Au<sub>4</sub>Cl<sub>4</sub>N<sub>8</sub>O<sub>24</sub> (3383.50): C, 41.18; H, 3.93; N, 3.31. Found: C, 41.35; H, 3.87; N, 3.33. IR (cm<sup>-1</sup>): ν(C=O) 1718 (*sh*); 1676 (*m*). <sup>1</sup>H NMR (CD<sub>2</sub>Cl<sub>2</sub>, 300.13 MHz, -40°C): δ 9.74 (*d*, <sup>4</sup>J<sub>H-H</sub> = 3.0 Hz, 1H, H<sup>2a</sup>), 9.49 (*d*, <sup>4</sup>J<sub>H-H</sub> = 3.0 Hz, 1H, H<sup>2b</sup>), 8.04 (*d*, <sup>3</sup>J<sub>H-H</sub> = 8.2 Hz, 1H, H<sup>5a</sup>), 7.57 (*d*, <sup>3</sup>J<sub>H-H</sub> = 7.8 Hz, 1H, H<sup>6a</sup>), 7.45 (*s*, 1H, H<sup>8</sup>), 7.42 (*s*, 1H, H<sup>8</sup>), 7.21 (*d*, <sup>3</sup>J<sub>H-H</sub> = 8.2 Hz, 1H, H<sup>5b</sup>), 7.13 (*d*, <sup>3</sup>J<sub>H-H</sub> = 7.8 Hz, 1H, H<sup>6b</sup>), 4.97 (*s*, 1H, H<sup>10</sup>), 2.53 (*s*, 3H, H<sup>12b</sup>), 2.06 (*s*, 3H, H<sup>12a</sup>), 1.35 (*s*, 9H, <sup>t</sup>Bu<sup>a</sup>), 0.81 (*s*, 9H, <sup>t</sup>Bu<sup>b</sup>). <sup>1</sup>H NMR (CD<sub>2</sub>Cl<sub>2</sub>, 300.13 MHz, 40°C): δ 9.69 (*bs*, 2H, H<sup>2</sup>), 7.73 (*bs*, 2H, H<sup>5a,6a</sup>), 7.57 (*bs*, 2H, H<sup>8a,8b</sup>), 7.39 (*bs*, 2H, H<sup>5b,6b</sup>), 4.95 (*s*, 1H, H<sup>10</sup>), 2.33 (*bs*, 6H, H<sup>12</sup>), 1.19 (*s*, 18H, <sup>t</sup>Bu). <sup>13</sup>C{<sup>1</sup>H} NMR the low solubility precludes its characterization by <sup>13</sup>C NMR.

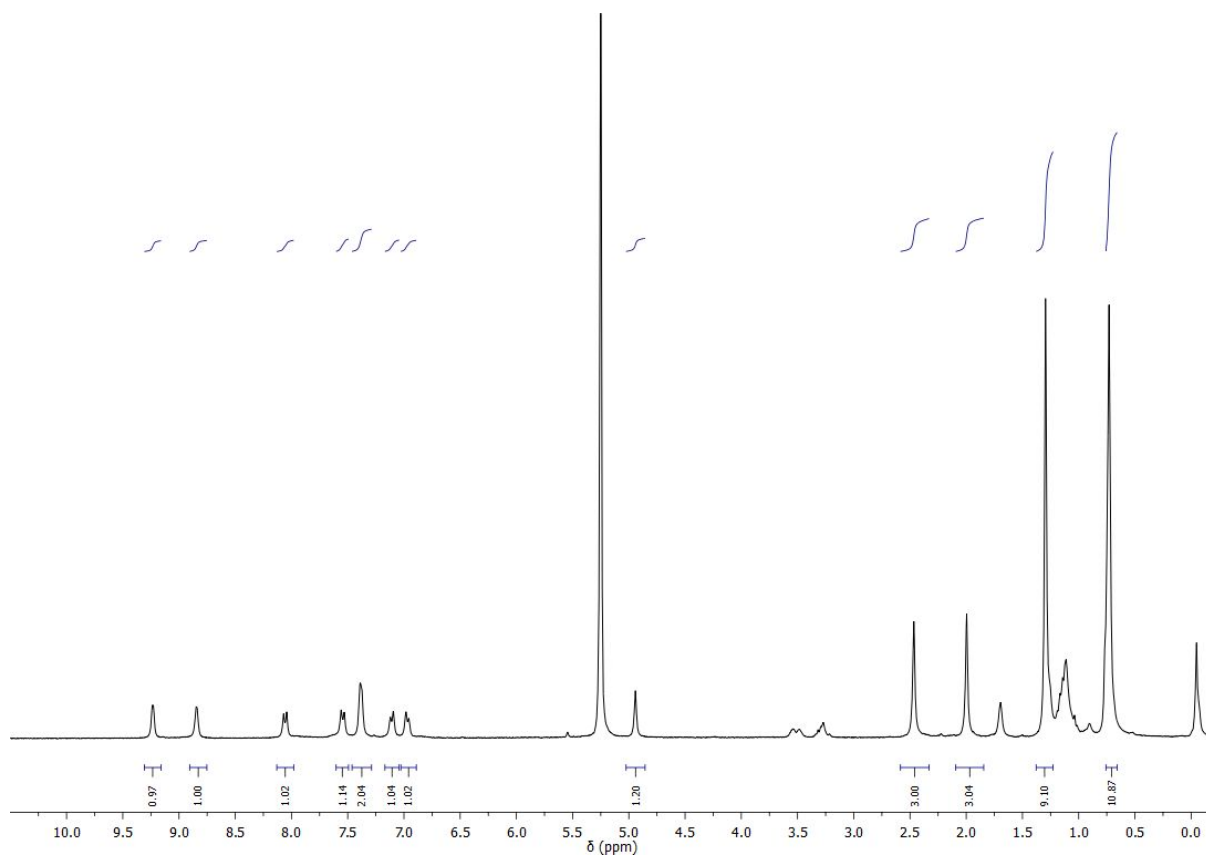


**Figure S1.4.**  $^1\text{H}$  NMR spectrum of  $3\text{SbF}_6$  at  $-40^\circ\text{C}$

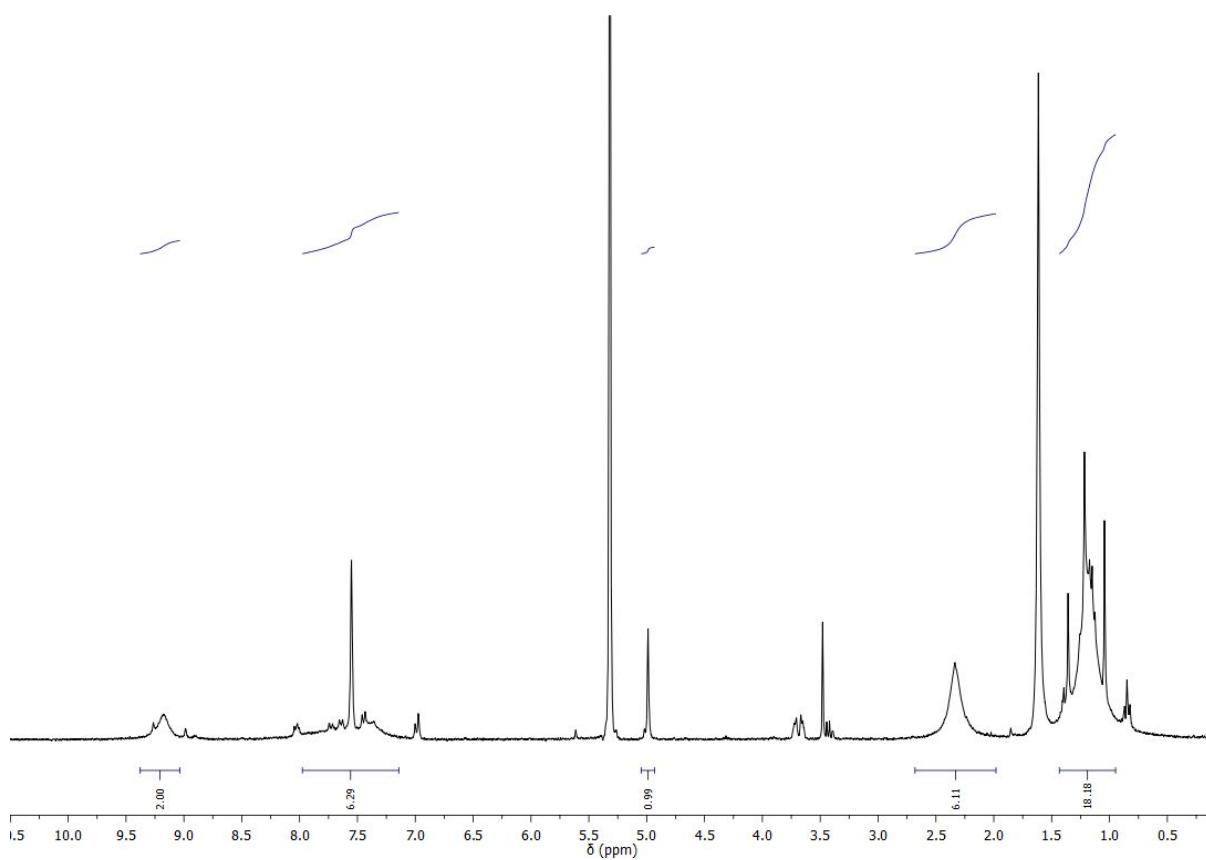


**Figure S1.5.**  $^1\text{H}$  NMR spectrum of  $3\text{SbF}_6$  at  $25^\circ\text{C}$ .

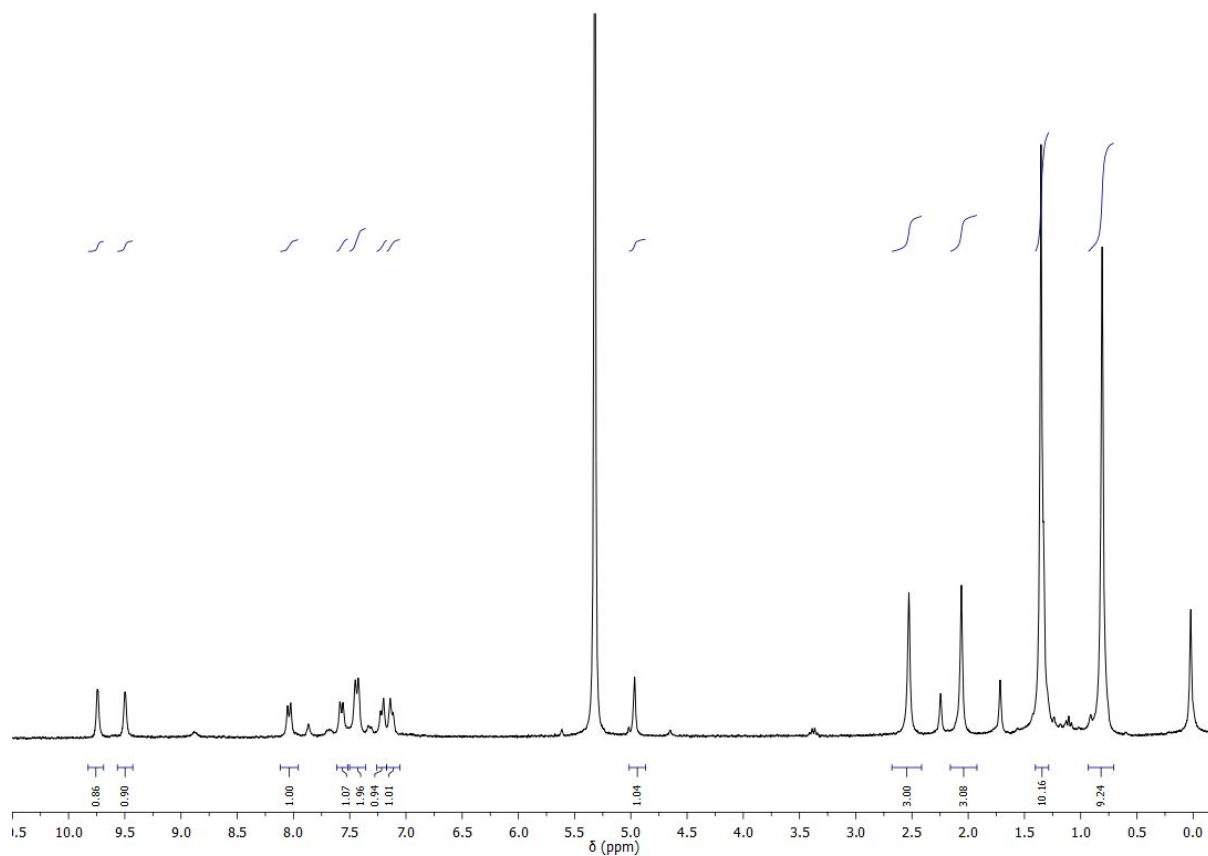


**Figure S1.6.** <sup>1</sup>H NMR spectrum of **3ClO<sub>4</sub>** at -40 °C.

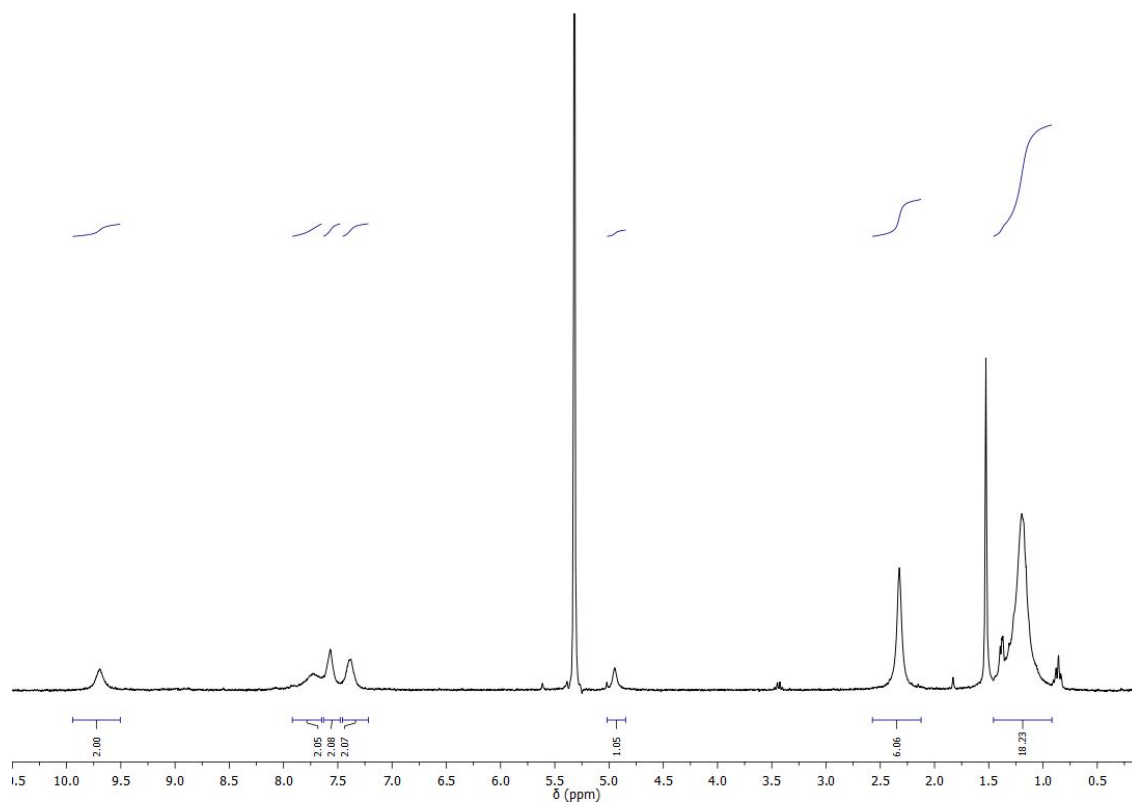
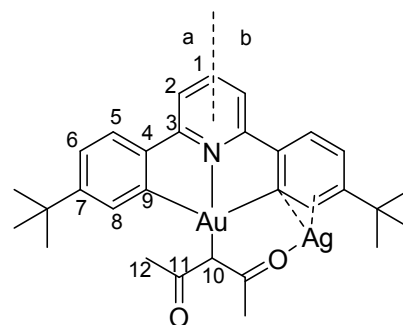


**Figure S1.7.** <sup>1</sup>H NMR spectrum of **3ClO<sub>4</sub>** at 40 °C.



**$[\{(C^{\wedge}N^{py^{\wedge}}C)Au(acac)\}_2Ag](SbF_6)_4$**

Under nitrogen, a  $CH_2Cl_2$  solution (c.a. 10 mL) of  $(C^{\wedge}N^{pz^{\wedge}}C)Au(acac)$  (20 mg, 0.03 mmol) was treated with  $AgSbF_6$  (21.6 mg, 0.06 mmol). This caused a color change from light-yellow to yellow. The solution was filtered through Celite and the solvent was evaporated. The yellow residue was precipitated with light petroleum, filtered off



and dried in air to give the pure product as a yellow powder (22.5 mg, 0.014 mmol, 93 % yield). Anal. Calcd for  $C_{60}H_{68}AgAu_2F_6N_2O_4Sb$  (1618.8): C, 44.52; H, 4.23; N, 1.73. Found: C, 44.15; H, 4.36; N, 1.50. IR ( $cm^{-1}$ ):  $\nu(C=O)$  1680 (m), 1669 (m).  $^1H$  NMR ( $CD_2Cl_2$ , 300.13 MHz,  $-40^\circ C$ ):  $\delta$  8.20 (m, 1H,  $H^1$ ), 7.72 (m, 2H,  $H^{2a+2b}$ ), 7.41-7.32 (m, 4H, aromatic), 6.70 (bd, 1H,  $H^{5a}$ ), 6.59 (bd, 1H,  $H^{5b}$ ), 4.90 (s, 1H,  $H^{10}$ ), 2.48 (s, 3H,  $H^{12a}$ ), 2.02 (s, 3H,  $H^{12b}$ ), 1.32 (s, 9H,  $tBu^a$ ), 0.71 (s, 9H,  $tBu^b$ ).  $^1H$  NMR ( $CD_2Cl_2$ , 300.13 MHz,  $25^\circ C$ ):  $\delta$  7.94 (t,  $^3J_{H-H} = 8.0$  Hz, 1H,  $H^1$ ), 7.50 (bs, 2H,  $H^8$ ), 7.44 (d,  $^3J_{H-H} = 8.0$  Hz, 2H,  $H^2$ ), 7.34 (d,  $^3J_{H-H} = 8.0$  Hz, 2H,  $H^5$ ), 7.22 (bd,  $J \sim 7.9$  Hz, 2H,  $H^6$ ), 4.79 (s, 1H,  $H^{10}$ ), 2.20 (s, 6H,  $H^{12}$ ), 1.23 (s, 18H,  $tBu$ ).  $^{13}C\{^1H\}$  NMR ( $CD_2Cl_2$ , 75.48 MHz): the low solubility precludes its characterization by  $^{13}C$  NMR.

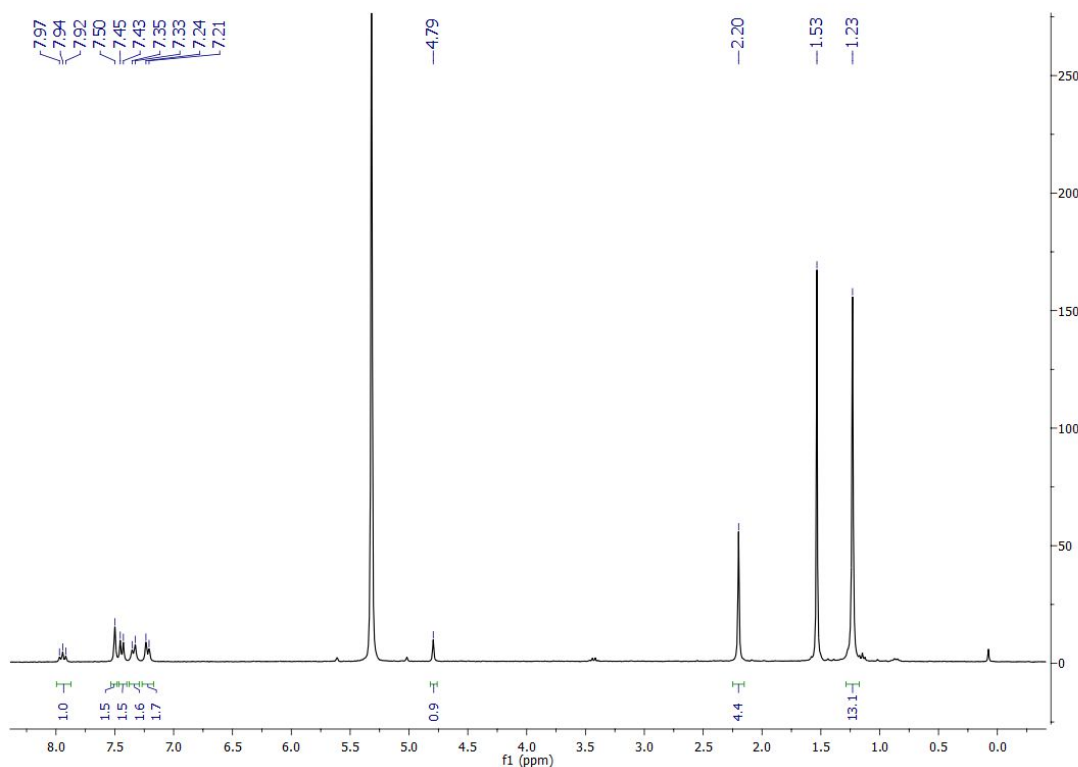


**Figure S1.8.**  $^1H$  NMR spectrum at  $25^\circ C$  of  $4SbF_6$

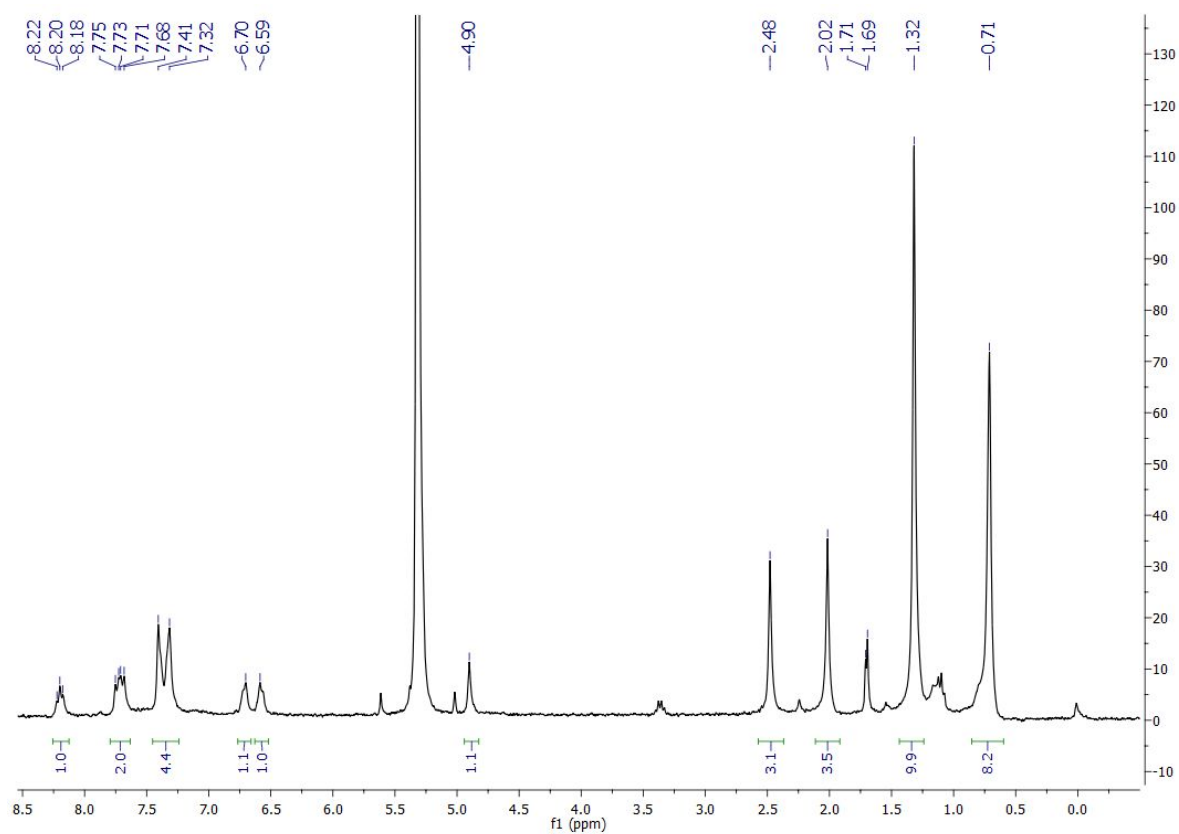


**Figure S1.9.**  $^1\text{H}$  NMR spectrum at  $-40^\circ\text{C}$  of  $4\text{SbF}_6$

**$\{[(C^{\wedge}N^{pz^{\wedge}}C)Au(malononitrile)_2]_2Ag(THF)](SbF_6)\}_n 5SbF_6$**

A THF (c.a. 10 mL) solution of  $(C^{\wedge}N^{pz^{\wedge}}C)Au(malonitrile)_2$  (25.0 mg, 0.04 mmol) was treated with  $AgSbF_6$  (6.9 mg, 0.02 mmol). The solution was stirred for 20 min, the solvent evaporated to dryness and the orange residue washed with light petroleum to give **5SbF<sub>6</sub>** as an orange powder (27.6 mg, 0.017 mmol, 87 % yield). Anal. Calcd for  $C_{54}H_{54}AgAu_2F_6N_8Sb + C_4H_8O$  (1624.7): C, 42.88; H, 3.85; N, 6.90. Found: C, 43.05; H, 3.94; N, 6.89. IR (cm<sup>-1</sup>):  $\nu(C \equiv N)$  2300 (w), 2240 (w). The complex shows poor solubility in non-coordinating solvents, while donor solvents dissolve the polymer by breaking it and therefore the NMR spectra are similar to the starting material.

**$\{[(C^{\wedge}N^{pz^{\wedge}}C)Au(malononitrile)_2]_2Ag(ClO_4)]\}_n 5ClO_4$**

The complex was made from  $(C^{\wedge}N^{pz^{\wedge}}C)Au(malonitrile)$  (25.0 mg, 0.04 mmol) and  $AgClO_4$  (4.1 mg, 0.02 mmol) following the method given for **5SbF<sub>6</sub>** as an orange powder (25.3 mg, 0.018 mmol, 89% yield). Anal. Calcd for  $C_{54}H_{54}AgAu_2ClN_8O_4$  (1416.3): C, 45.79; H, 3.84; N, 7.91. Found: C, 46.10; H, 4.03; N, 7.70. IR (cm<sup>-1</sup>):  $\nu(C \equiv N)$  2267 (w); 2240 (w). The complex shows poor solubility in non-coordinating solvents, while donor solvents dissolve the polymer by breaking it up; and, therefore the NMR spectra are similar to the starting material.

## S2. X-ray crystallography

Crystals were mounted in MiTeGen MicroMesh systems and fixed on the diffractometer in a cold nitrogen stream. Diffraction intensities were recorded at low temperature using an Oxford Diffraction Xcalibur-3/Sapphire3-CCD diffractometer, equipped with Mo-K $\alpha$  radiation and graphite monochromator or a Rigaku HG Saturn724+ (2 $\times$ 2 bin mode). Data were processed using the CrystAlisPro-CCD and –RED software or CrystalClear-SM Expert 3.1 b27, with the absorption correction done at this stage.<sup>S1</sup>

The structures of all samples were determined by the direct methods routines with SHELXS or SHELXT programs and refined by full-matrix least-squares methods on F<sup>2</sup> in SHELXL.<sup>S2</sup> Non-hydrogen atoms were generally refined with anisotropic thermal parameters. Hydrogen atoms were included in idealized positions. No missed symmetry was reported by PLATON.<sup>S3</sup>

Refinement results are included in Table S1. Computer programs used in this analysis were run through WinGX.<sup>S4</sup> Scattering factors for neutral atoms were taken from reference S5.

### Crystallographic details

$[(C^{N^{tBu}}C)AuCN]_2Ag_2[SbF_6]_2 \cdot 3 CH_2Cl_2$  **2SbF<sub>6</sub>**  $\cdot 3 CH_2Cl_2$ : Clear light yellow prism (0.20 $\times$ 0.10 $\times$ 0.10) grown by slow diffusion in two layers CH<sub>2</sub>Cl<sub>2</sub>:pentane (1:2) at room temperature. The asymmetric unit corresponds to two trinuclear [Au<sub>2</sub>Ag] units bonded through Ag $\cdots$ Ag interaction and 3 molecules of CH<sub>2</sub>Cl<sub>2</sub>. OMIT instruction was used to remove some particularly disagreeable reflections. Some positional restraints had to be introduced to model the SbF<sub>6</sub> group. Several peaks higher than 1 e. $\text{\AA}^{-3}$  were found next to the Au centers without any chemical meaning but this causes 3 A-alerts in the Checkcif.

$[(C^{N^{tBu}}C)AuCN]_2Ag[ClO_4] \cdot 1.5 CH_2Cl_2$  **2ClO<sub>4</sub>**  $\cdot 1.5 CH_2Cl_2$ : Clear light yellow prism (0.15 $\times$ 0.12 $\times$ 0.05) grown by slow diffusion in two layers CH<sub>2</sub>Cl<sub>2</sub>:pentane (1:2) at room temperature. The asymmetric unit corresponds to one trinuclear [Au<sub>2</sub>Ag] unit and two molecules of CH<sub>2</sub>Cl<sub>2</sub> one of which shows 50% occupancy. OMIT instruction was used to remove some particularly disagreeable reflections. Several peaks higher than 1 e. $\text{\AA}^{-3}$  were found next to the heavy atoms without any chemical meaning but this causes 1 A-alert in the Checkcif.

$[\{(C^{N^{pz}}C)Au(acac)\}_2Ag]_2\{Ag(SbF_6)_4\} \cdot 6 C_7H_8$  **3SbF<sub>6</sub>**  $\cdot 6 C_7H_8$ : Clear gold block (0.25 $\times$ 0.1 $\times$ 0.05) grown by slow evaporation of a solution of the crude solid in CH<sub>2</sub>Cl<sub>2</sub>:Toluene (1:5) at room temperature. The asymmetric unit corresponds to one half of

the octanuclear aggregate and two molecules of toluene. In addition, the use of SQUEEZE reveals the presence of voids and electron density that fits well with the presence of 4 additional toluene molecules per unit cell. OMIT instruction was used to remove some particularly disagreeable reflections. Some positional restrains had to be introduced to model the  $\text{SbF}_6$  group and the solvent molecules. Some atoms were refined introducing the ISOR restrain. Several peaks higher than  $1 \text{ e.}\text{\AA}^{-3}$  were found next to the Au centers without any chemical meaning.

$[\{(\text{C}^{\text{N}^{\text{pz}}}\text{C})\text{Au}(\text{acac})\}_2\text{Ag}\}_2\{\text{Ag}(\text{ClO}_4)_4\}] \cdot 1.5 \text{ CH}_2\text{Cl}_2 \cdot 2 \text{ C}_5\text{H}_{12} \text{ 3ClO}_4 \cdot 1.5 \text{ CH}_2\text{Cl}_2 \cdot 2 \text{ C}_5\text{H}_{12}$ : Orange block ( $0.2 \times 0.1 \times 0.1$ ) grown by slow diffusion of pentane in a saturated solution of the crude material in  $\text{CH}_2\text{Cl}_2$  at room temperature. The asymmetric unit corresponds to one half of the octanuclear aggregate a  $\text{CH}_2\text{Cl}_2$  with occupancy of 75% and one pentane. The pentane molecule was refined in isotropic. Some positional and ISOR restrains were introduced to model some parts of the molecule and the solvent. Several peaks higher than  $1 \text{ e.}\text{\AA}^{-3}$  were found next to the Au centers without any chemical meaning. The check-cif reveals one A-alert due to a solvent accessible VOID of  $268 \text{ \AA}^3$ . Most likely, this void is occupied by solvent but it could not be model.

$[\{(\text{C}^{\text{N}^{\text{py}}}\text{C})\text{Au}(\text{acac})_2\}_2\text{Ag}]\text{(SbF}_6\text{)} \cdot \text{CH}_2\text{Cl}_2 \text{ 4SbF}_6 \cdot \text{CH}_2\text{Cl}_2$ : Yellow needle ( $0.8 \times 0.1 \times 0.05$ ) grown by slow evaporation of a solution of the crude material in  $\text{CH}_2\text{Cl}_2$  at room temperature. The asymmetric unit corresponds to the complex and one molecule of  $\text{CH}_2\text{Cl}_2$  that is disordered between two positions. Some EADP restrictions were used to model the disorder in the solvent. Several peaks higher than  $1 \text{ e.}\text{\AA}^{-3}$  were found next to the Au centers without any chemical meaning. One particularly big peak very close to one Au atom causes a A-alert indicating that the crystal might been moved during the experiment.

$\{[\{(\text{C}^{\text{N}^{\text{pz}}}\text{C})\text{Au}(\text{malonitrile})_2\}_2\text{Ag}(\text{THF})]\text{(SbF}_6\text{)}\}_n \text{ 5SbF}_6$ : Orange block ( $0.10 \times 0.10 \times 0.05$ ) grown by slow evaporation of a THF solution at room temperature. The asymmetric unit corresponds to one half of the fragment that defines the complex. Several peaks higher than  $1 \text{ e.}\text{\AA}^{-3}$  were found in the vicinity of the Au center without any chemical meaning.

**Table S2.1.** Selected crystal data and structure refinement details for:

|   | <b>2SbF<sub>6</sub> · 3 CH<sub>2</sub>Cl<sub>2</sub></b>   | <b>2ClO<sub>4</sub> · 3 CH<sub>2</sub>Cl<sub>2</sub></b>   | <b>3SbF<sub>6</sub> · 6 C<sub>7</sub>H<sub>8</sub></b>  |
|---|--|--|---|
| Empirical formula   | C <sub>123</sub> H <sub>146</sub> Ag <sub>2</sub> Au <sub>4</sub> Cl <sub>6</sub> F <sub>12</sub> N <sub>8</sub> Sb <sub>2</sub> | C <sub>125</sub> H <sub>148</sub> Ag <sub>2</sub> Au <sub>4</sub> C <sub>112</sub> N <sub>8</sub> O <sub>8</sub> | C <sub>144</sub> H <sub>164</sub> Ag <sub>4</sub> Au <sub>4</sub> F <sub>24</sub> N <sub>8</sub> O <sub>8</sub> Sb <sub>4</sub> |
| <i>F</i> <sub>w</sub>   | 3424.28  | 3319.54  | 4297.17   |
| T (K)   | 140(2)   | 100(2)   | 100(2)  |
| crystal system, space group   | Triclinic, P-1   | Triclinic, P-1   | Monoclinic, P2 <sub>1</sub> /c  |
| a(Å)  | 14.4842(5)   | 15.5836(4)   | 14.7873(4)  |
| b(Å)  | 17.8164(7)   | 15.7831(2)   | 29.1044(7)  |
| c(Å)  | 24.8141(9)   | 16.3589(3)   | 20.7307(8)  |
| α(deg)  | 89.310(3)  | 91.5680(10)  | 90  |
| β(deg)  | 80.005(3)  | 117.614(2)   | 106.213(4)  |
| γ(deg)  | 84.500(3)  | 110.334(2)   | 90  |
| volume (Å <sup>3</sup> )  | 6277.1(4)  | 3255.98(13)  | 8567.2(5)   |
| Z   | 2  | 1  | 2   |
| <i>D</i> <sub>calcd</sub> (Mg/m <sup>3</sup> )  | 1.812  | 1.693  | 1.666   |
| absorption coefficient (mm <sup>-1</sup> )  | 5.579  | 5.086  | 4.551   |
| F(000)  | 3324   | 1632   | 4144  |
| θ range for data collection (°)   | 3.138 to 29.964  | 1.775 to 27.484  | 2.425 to 26.372   |
| data // restraints // params  | 25630 // 3 // 1414   | 14932 // 0 // 748  | 17516 // 54 // 838  |
| goodness-of-fit on F <sup>2</sup> [a]   | 1.057  | 1.055  | 1.062   |
| final R indexes [I>2σ(I)] <sup>[a]</sup>  | R1 = 0.0467, wR2 = 0.1199  | R1 = 0.0322, wR2 = 0.0793  | R1 = 0.0988, wR2 = 0.2535   |
| R indexes (all data) <sup>[a]</sup>   | R1 = 0.0681, wR2 = 0.1319  | R1 = 0.0365, wR2 = 0.0818  | R1 = 0.1261, wR2 = 0.2674   |
| largest diff peak and hole (e.Å <sup>-3</sup> )   | 3.565 and -2.875   | 3.766 and -3.066   | 5.805 and -4.621  |
| <sup>[a]</sup> $R1 = \Sigma( F_o  -  F_c )/\Sigma F_o $ ; $wR2 = [\Sigma w(F_o^2 - F_c^2)^2/\Sigma wF_o^2]^{1/2}$ ; goodness of fit = $\{\Sigma[w(F_o^2 - F_c^2)^2]/(N_{\text{obs}} - N_{\text{param}})\}^{1/2}$ ; $w = [\sigma^2(F_o) + (g_1P)^2 + g_2P]^{-1}$ ; $P = [\max(F_o^2; 0 + 2F_c^2)]/3$ . |  |  |   |

**Table S2.1 Continued.** Selected crystal data and structure refinement details for:

|  | <b>3ClO<sub>4</sub> · 1.5 CH<sub>2</sub>Cl<sub>2</sub> · 2 C<sub>5</sub>H<sub>12</sub></b>                              | <b>4SbF<sub>6</sub> · CH<sub>2</sub>Cl<sub>2</sub></b>  | <b>5SbF<sub>6</sub></b>   |
|--|---|---|---|
| Empirical formula                                  | C <sub>63.75</sub> H <sub>79.50</sub> Ag <sub>2</sub> Au <sub>2</sub> Cl <sub>3.50</sub> N <sub>4</sub> O <sub>12</sub> | C <sub>61</sub> H <sub>70</sub> AgAu <sub>2</sub> Cl <sub>2</sub> F <sub>6</sub> N <sub>2</sub> O <sub>4</sub> S<br>b | C <sub>29</sub> H <sub>30</sub> Ag <sub>0.50</sub> AuF <sub>3</sub> N <sub>4</sub> O <sub>0.50</sub> Sb <sub>0.50</sub> |
| <i>F</i> <sub>w</sub>                              | 1827.56   | 1703.66   | 811.34  |
| T (K)  | 140(2)  | 140(2)  | 140(2)  |
| crystal system,<br>space group                     | Monoclinic, P2 <sub>1</sub> /n  | Monoclinic, P2 <sub>1</sub> /n  | Monoclinic, P2/c  |
| a(Å)   | 15.2738(3)  | 11.3004(4)  | 9.9253(2)   |
| b(Å)   | 28.5808(5)  | 19.2339(10)   | 13.5829(4)  |
| c(Å)   | 17.4532(3)  | 28.4550(11)   | 21.2428(4)  |
| α(deg)   | 90  | 90  | 90  |
| β(deg)   | 105.386(2)  | 93.907(3)   | 92.194(2)   |
| γ(deg)   | 90  | 90  | 90  |
| volume (Å <sup>3</sup> )                           | 7345.9(2)   | 6170.3(5)   | 2861.74(12)   |
| Z  | 4   | 4   | 4   |
| <i>D</i> <sub>calcd</sub> (Mg/m <sup>3</sup> )     | 1.652   | 1.834   | 1.883   |
| absorption<br>coefficient (mm <sup>-1</sup> )      | 4.691   | 5.637   | 5.981   |
| F(000)   | 3590  | 3304  | 1564  |
| θ range for data<br>collection (°)                 | 2.857 to 30.052   | 3.44 to 31.886  | 3.273 to 28.686   |
| data // restraints //<br>params                    | 19670 // 11 // 765  | 14134 // 0 // 766   | 6643 // 12 // 356   |
| goodness-of-fit on<br>F <sup>2</sup> [a]           | 1.028   | 1.059   | 0.954   |
| final R indexes<br>[I > 2σ(I)] <sup>[a]</sup>      | R1 = 0.0538, wR2 = 0.1107   | R1 = 0.051, wR2 = 0.1051  | R1 = 0.0452, wR2 = 0.0636   |
| R indexes (all<br>data) <sup>[a]</sup>             | R1 = 0.0842, wR2 = 0.1207   | R1 = 0.0733, wR2 =<br>0.1183  | R1 = 0.0802, wR2 = 0.0717   |
| largest diff peak<br>and hole (e.Å <sup>-3</sup> ) | 2.968 and -1.312  | 6.76 and -2.585   | 2.355 and -1.452  |

<sup>[a]</sup>  $R1 = \Sigma(|F_o| - |F_c|)/\Sigma|F_o|$ ;  $wR2 = [\Sigma w(F_o^2 - F_c^2)/\Sigma wF_o^2]^{1/2}$ ; goodness of fit =  $\{\Sigma[w(F_o^2 - F_c^2)^2]/(N_{\text{obs}} - N_{\text{param}})\}^{1/2}$ ;  $w = [\sigma^2(F_o) + (g_1P)^2 + g_2P]^{-1}$ ;  $P = [\max(F_o^2, 0) + 2F_c^2]/3$ .

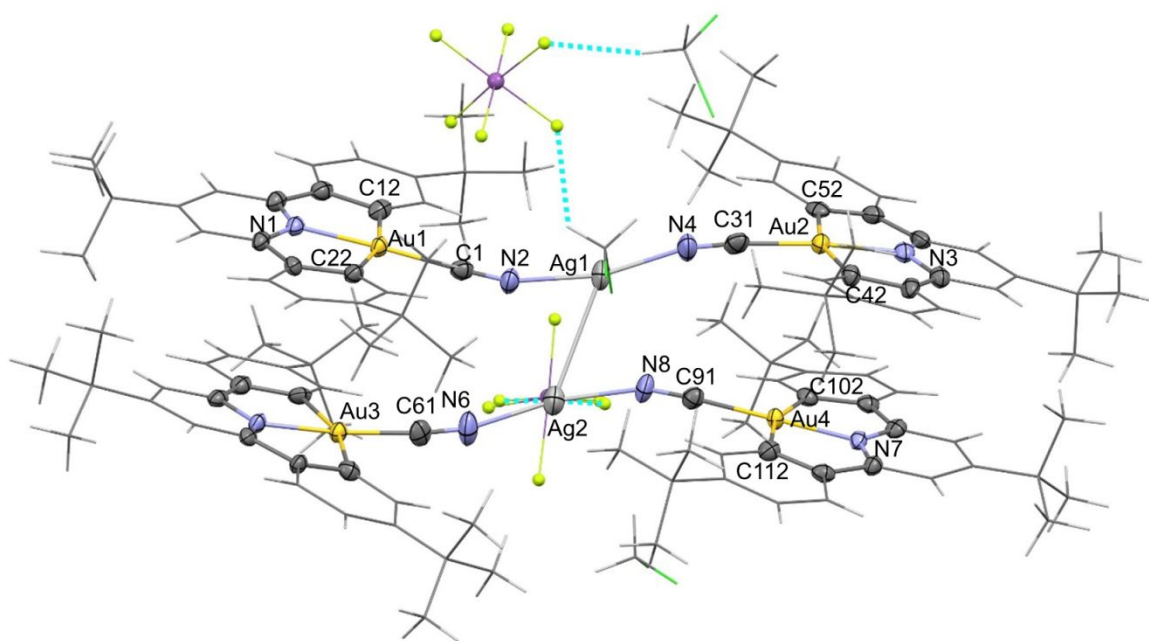


**Figure S2.1.** View of the X-ray structure of  $[\{(C^N^{tBu^C})AuCN\}_2Ag]_2[SbF_6]_2 \cdot 3 CH_2Cl_2$ . The structure is shown as stick-based skeleton with only the most relevant atoms represented as ellipsoids with 50% probability level. Selected bond distances (Å) and angles (°): Au1-C1 1.975(8), C1-N2 1.13(1), N2-Ag1 2.104(7), Au2-C31 1.964(8), C31-N4 1.15(1), N4-Ag1 2.087(8), Au3-C61 1.969(8), C61-N6 1.13(1), N6-Ag2 2.105(8), Au4-C91 1.974(7), C91-N8 1.15(1), N8-Ag2 2.127(7), Ag1-Ag2 3.103(1), Au1-C1-N2 177.7(7), C1-N2-Ag1 162.8(6), Au2-C31-N4 173.6(7), C31-N4-Ag1 165.6(7), N2-Ag1-N4 165.7(3), Au3-C61-N6 171.8(7), C61-N6-Ag2 167.5(7), Au4-C91-N8 177.1(7), C91-N8-Ag2 161.2(6), N6-Ag2-N8 160.2(3).



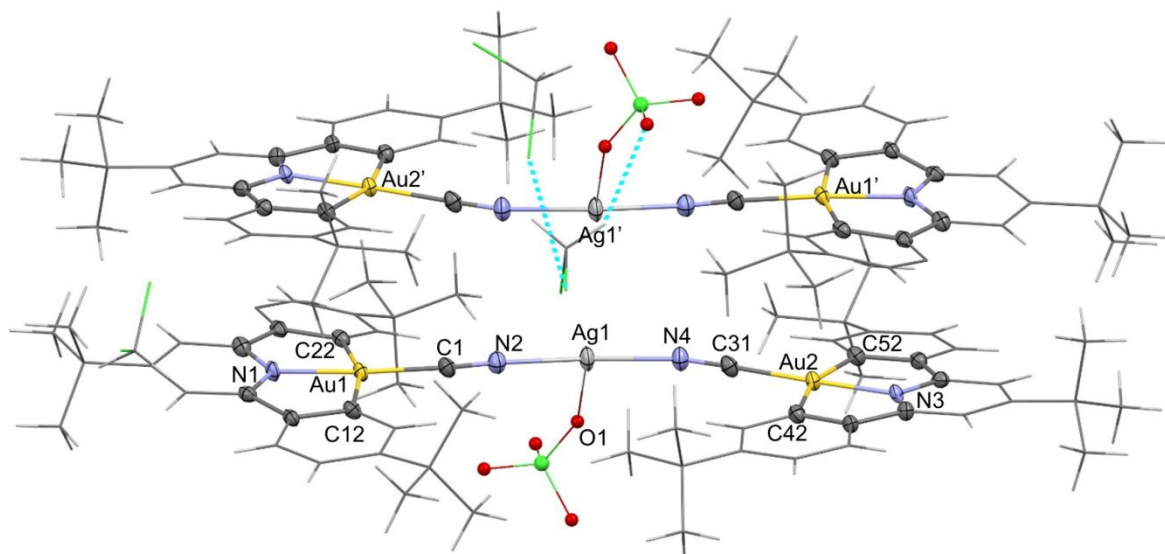


**Figure S2.2.** View of the X-ray structure of  $[\{(C^N{}^{tBu}C)AuCN\}_2Ag]_2[SbF_6]_2 \cdot 3 CH_2Cl_2 \cdot 2ClO_4 \cdot 3 CH_2Cl_2$ . The structure is shown as stick-based skeleton with only the most relevant atoms represented as ellipsoids with 50% probability level. Selected bond distances (Å) and angles (°): Au1-C1 1.956(6), C1-N2 1.149(8), N2-Ag1 2.097(6), Au2-C31 1.969(6), C31-N4 1.138(8), N4-Ag1 2.102(6), Ag1-O1 2.584(4), Ag1-Ag1' 3.3881(5), Au1-C1-N2 175.6(4), C1-N2-Ag1 174.6(4), Au2-C31-N4 176.2(4), C31-N4-Ag1 168.8(4), N2-Ag1-N4 161.8(2), N2-Ag1-O1 96.3(2), N4-Ag1-O1 97.4(2).

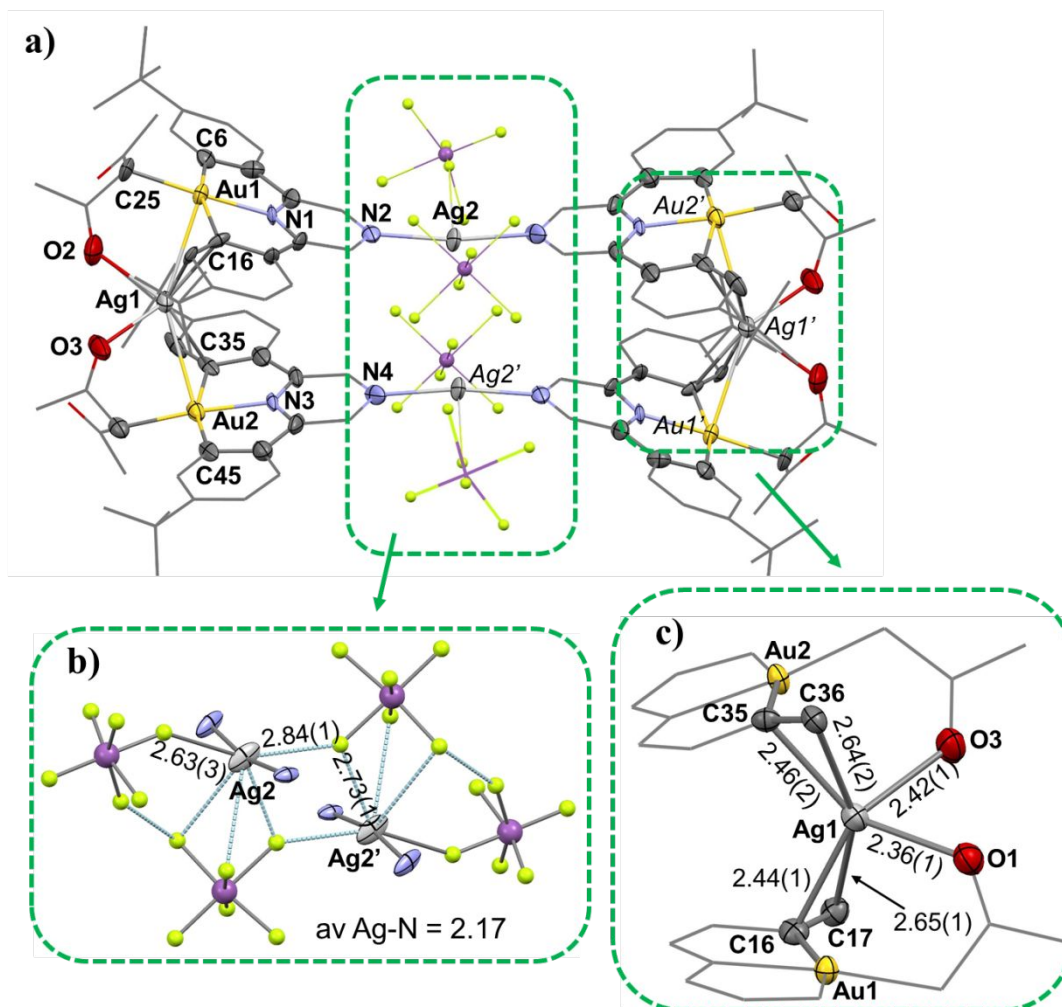


**Figure S2.3.** (a) View of the X-ray structure of  $[ \{ \{ (C^{\wedge}N^{pz}C)Au(acac) \}_2 Ag_2 \} \{ Ag(SbF_6)_4 \} ] \cdot 6 C_7H_8 \cdot 3 SbF_6 \cdot 6 C_7H_8$ . Shown as stick-based skeleton with only the most relevant atoms represented as ellipsoids with 50% probability level. Selected bond distances (Å) and angles (°): Au1-C25 2.09(2), Au1-C6 2.08(2), Au1-C16 2.12(1), Au1-N1 2.00(1), Au2-C35 2.11(2), Au2-C45 2.05(2), Au2-C54 2.06(2), Au2-N3 2.02(1), Ag1-O2 2.36(1), Ag1-O3 2.42(2), Ag1-C16 2.44(1), Ag1-C17 2.65(1), Ag1-C35 2.46(2), Ag1-C36 2.64(2), Ag2-N2 2.19(1), Ag2-N4' 2.16(2), Ag2-F7 2.63(3), Ag2-F2 2.84(1), Ag2-F2' 2.73(1), C6-Au1-N1 80.6(5), C16-Au1-N1 80.5(5), C16-Au1-C25 102.5(6), C6-Au1-C25 102.5(6), C6-Au1-C16 160.9(6), N1-Au1-C25 176.9(6), C35-Au2-N3 79.6(5), C45-Au2-N3 81.5(5), C35-Au2-C54 103.6(6), C45-Au2-C54 95.4(6), C45-Au2-C35 161.0(6), N3-Au2-C54 174.8(5), O2-Ag1-O3 79.9(5), O3-Ag1-centroid(C35-C36) 107.91, O2-Ag1-centroid(C35-C36) 113.67, centroid(C35-C36)-Ag1-centroid(C16-C17) 137.99, N2-Ag2-N4' 167.9(5), F2-Ag2-F7 157.4(6), F2-Ag2-F2' 67.4(3), Ag2-F2-Ag2' 112.6(3). (b) View in detail for the coordination environment of Ag2. (c) View in detail for the coordination environment of Ag1.

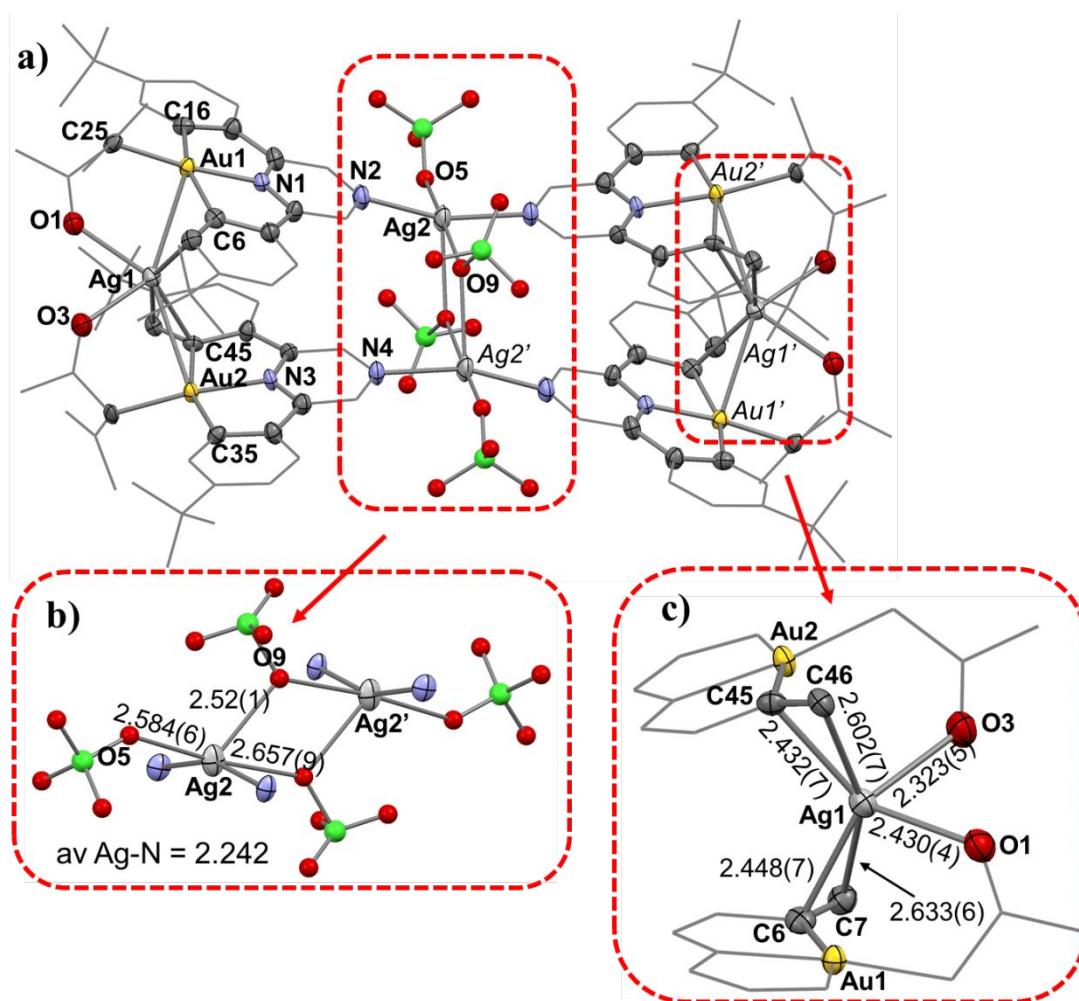


**Figure S2.4.** (a) View of the X-ray structure of  $[\{ \{ (C^N)^{pz}C \} Au(acac) \}_2 Ag_2 \{ Ag(ClO_4)_4 \}] \cdot 1.5 CH_2Cl_2 \cdot 2 C_5H_{12} \cdot 3 ClO_4 \cdot 1.5 CH_2Cl_2 \cdot 2 C_5H_{12}$ . The structure is shown as stick-based skeleton with only the most relevant atoms represented as ellipsoids with 50% probability level. Selected bond distances (Å) and angles (°): Au1-C25 2.070(6), Au1-C6 2.115(6), Au1-C16 2.077(6), Au1-N1 2.024(5), Ag1-O1 2.430(4), Ag1-O3 2.323(5), Ag1-C6 2.447(7), Ag1-C7 2.633(6), Ag1-C45 2.432(7), Ag-C46 2.602(7), Ag2-N2 2.244(6), Ag2-N4' 2.241(5), Ag2-O5 2.584(6), Ag2-O9 2.52(1), Ag2-O9' 2.657(9), C6-Au1-N1 80.1(2), C16-Au1-N1 80.6(2), C16-Au1-C25 95.8(2), C6-Au1-C25 103.7(2), C6-Au1-C16 160.3(2), N1-Au1-C25 174.0(2), O1-Ag1-O3 76.2(2), O1-Ag1-centroid(C45-C46) 111.00, O3-Ag1-centroid(C6-C7) 112.27, centroid(C6-C7)-Ag1-centroid(C45-C46) 134.84, N2-Ag2-N4' 158.6(2), O5-Ag2-O9' 174.5(2), O9-Ag2-O9' 61.0(3), Ag2-O9-Ag2' 119.0(4). (b) View in detail for the coordination environment of Ag2. (c) View in detail for the coordination environment of Ag1.

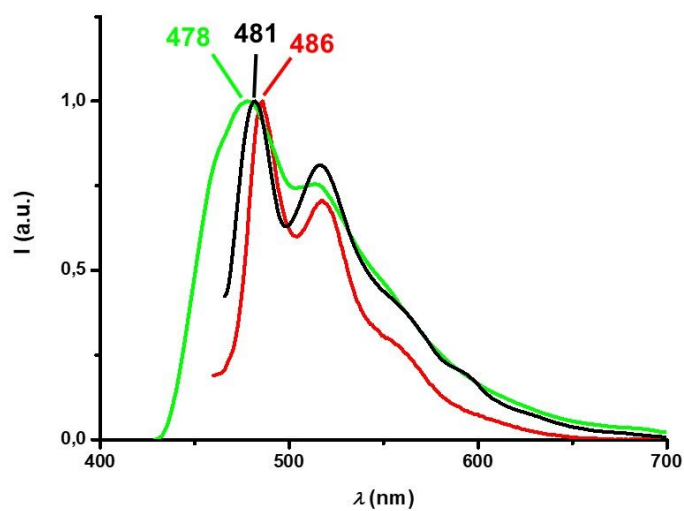


### S3. Photophysical Properties

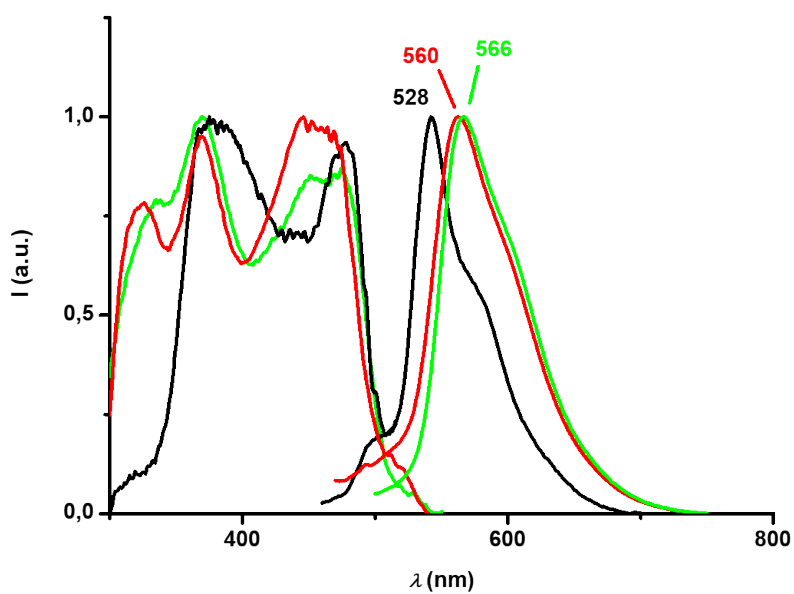
UV–visible absorption spectra were recorded using a Perkin-Elmer Lambda 35 UV/vis spectrometer. Excitation and emission spectra were measured using a (TCSPC) FluoroLog Horiba Jobin Yvon spectrofluorometer or an Acton Research Corporation Spectrapro 2500i 0.500m imaging triple grating monochromator/spectrograph. Lifetime measurements were conducted with a Datastation HUB-B with a nanoLED controller and software DAS6. The nanoLEDs employed for lifetime measurements were of 370 nm with pulse lengths of 0.8–1.4 ns. Quantum yields in the solid state were measured upon excitation at 370–400 nm using an F-3018 integrating sphere mounted on a Fluorolog 3-11 Tau-3 spectrofluorimeter. Polymeric sample preparation: PS (polystyrene) was purchased from commercial sources. Thin films were prepared by spin/drop casting from a solution of the corresponding complex and a sufficient amount of polymer to reach the desired concentration in each case. Films were then placed under vacuum for 10 minutes to remove residual solvent. In the cases of **1SbF<sub>6</sub>**, **1ClO<sub>4</sub>** and **5SbF<sub>6</sub>** and due to the low solubility of the materials an alternative approach was used, consisting on mixing the [Au] complexes with the right amount of the corresponding silver salts in a THF/PS mixture. This mixture was spin cast generated homogeneous films and was the preferred method for these preparations.

**Table S3.1:** Photophysical properties of the complexes in CH<sub>2</sub>Cl<sub>2</sub> (10<sup>-4</sup> M)

| Complex                   | Absorbance [nm] (10 <sup>3</sup> ε/M <sup>-1</sup> cm <sup>-1</sup> )             | λ <sub>em</sub> / nm (λ <sub>ex</sub> / nm)                          |  |
|---------------------------|---|--|--|
|                           |   | 298 K  | 77 K   |
| [ <sup>t</sup> Bu-pyAu]CN | 280 (22.7), 320 <sub>sh</sub> (15.8), 380 (4.0), 390 (4.8), 410 (5.2).            | a)   | 495 <sub>max</sub> , 523, 555 <sub>sh</sub> (320-410)                |
| 2SbF <sub>6</sub>         | 279 (20.2), 320 <sub>sh</sub> (19.0), 388 (4.2), 395 (3.6), 418 (6.5).            | 500 <sub>max</sub> , 535 <sub>sh</sub> (320-410)                     | 508 <sub>max</sub> , 528, 560 <sub>sh</sub> (320-410)                |
| 2ClO <sub>4</sub>         | 280 (22.0), 320 <sub>sh</sub> (16.2), 380 (3.9), 392 (5.0), 416 (5.5).            | 502 <sub>max</sub> , 537 <sub>sh</sub> (320-410)                     | 506 <sub>max</sub> , 526, 560 <sub>sh</sub> (320-410)                |
| [ <sup>p</sup> zAu]acac   | 293 (19.5), 319 (15.5), 340 <sub>sh</sub> (9.0), 399 (4.0), 419 (6.2), 442 (6.2). | 480, 522 (320-450)   | 540 <sub>max</sub> , 572 <sub>sh</sub> (320-420)                     |
| 3SbF <sub>6</sub>         | 319 (25.2), 368 (10.9), 424 (5.9), 450 (8.0), 476 (7.7).                          | 505 <sub>sh</sub> , 569 <sub>max</sub> , 600 <sub>sh</sub> (320-480) | 533 <sub>sh</sub> , 558 <sub>max</sub> , 598 <sub>sh</sub> (320-460) |
| 3ClO <sub>4</sub>         | 319 (16.5), 360 <sub>sh</sub> (9.0), 426 (4.8), 447 (7.2), 469 (7.3).             | 559 <sub>max</sub> , 592 <sub>sh</sub> , (320-480).                  | 544 <sub>max</sub> , 572 <sub>sh</sub> , (320-420).                  |
| [ <sup>p</sup> yAu]acac   | 281 (18.7), 318 <sub>sh</sub> (12.8), 379 (4.2), 389 (4.9), 408 (4.7).            | 445 (320-410)  | 490 <sub>max</sub> , 521, 550 <sub>sh</sub> (320-410)                |
| 4SbF <sub>6</sub>         | 281 (27.3), 318 <sub>sh</sub> (15.3), 370 (3.1), 395 (6.0), 413 (5.7).            | 408 <sub>sh</sub> , 442 <sub>max</sub> (320-420)                     | 499 <sub>max</sub> , 535, 562 <sub>sh</sub> (320-415)                |
| a) No emissive            |   |  |  |



**Figure S3.1:** Emission bands of complexes  $[\text{tBu-pyAu}]\text{CN}$  (black),  $2\text{SbF}_6$  (green), and  $2\text{ClO}_4$  (red) in PS at 298 K.

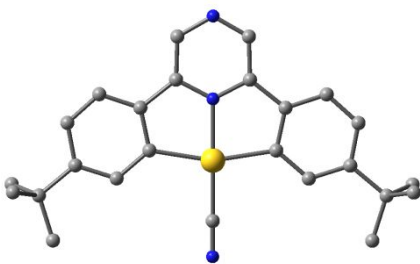
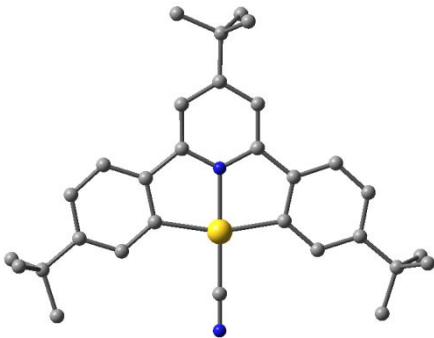
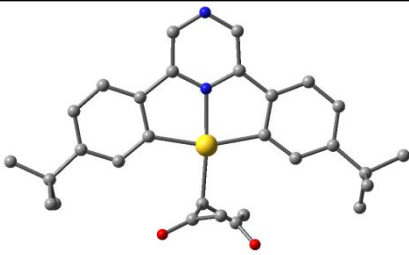
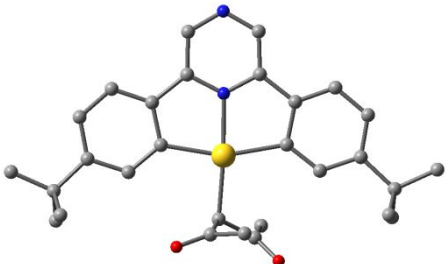


**Figure S3.2:** Emission and excitation bands of complexes  $[\text{pzAu}]\text{mln}$  (black),  $5\text{SbF}_6$  (green), and  $5\text{ClO}_4$  (red) in PS at 298 K.

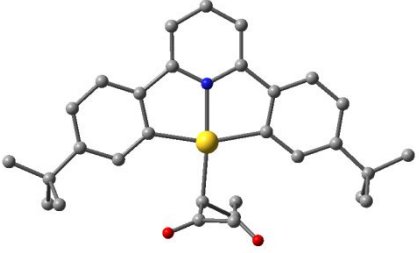
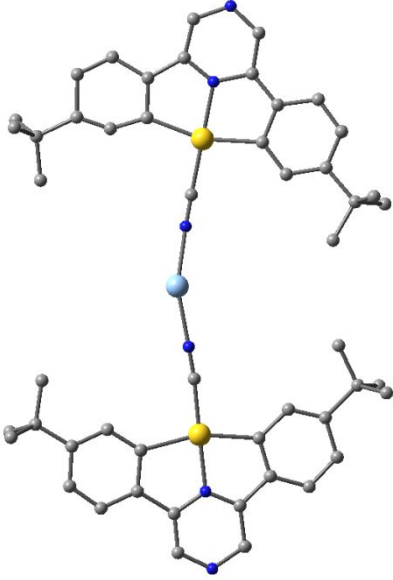
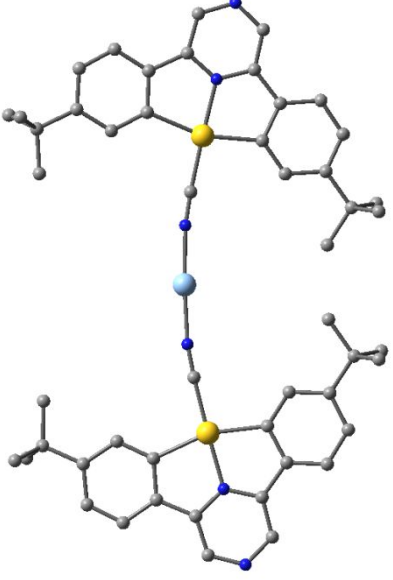
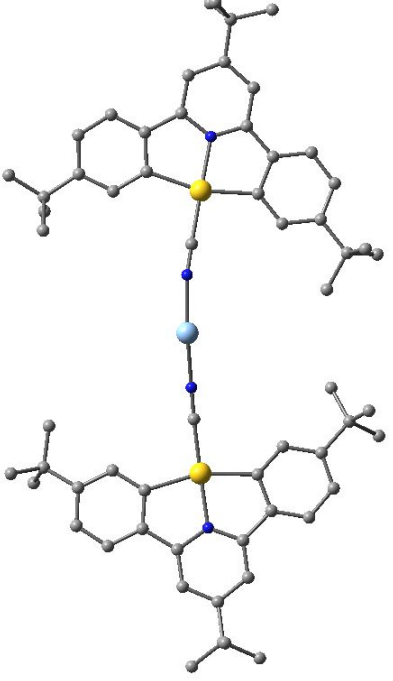
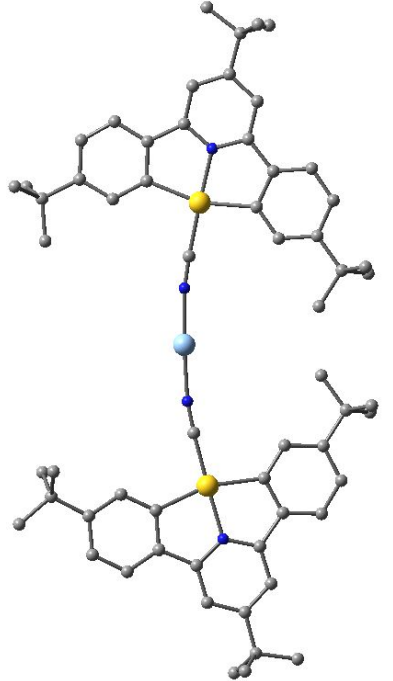
#### S4. Theoretical Calculations

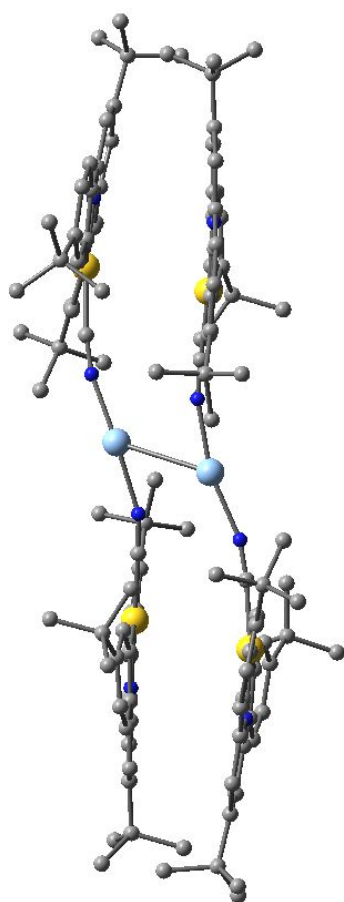
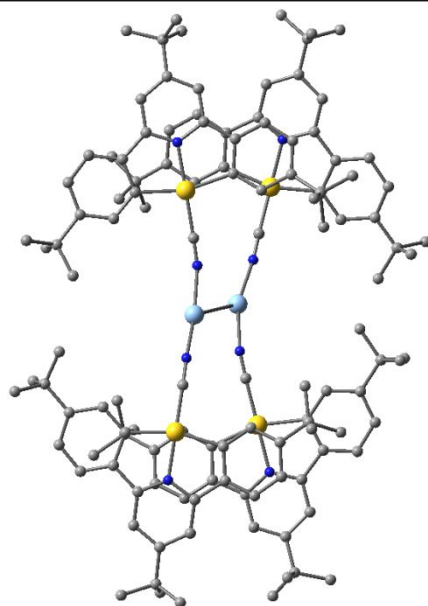
The ground states of the complexes were studied by density functional theory (DFT) and the S1 states by time-dependent DFT (TD-DFT) calculations.<sup>S6</sup> The structures of the [pzAu]CN and [pzAu]acac precursors were optimized. Other complexes were studied in crystal structure geometries. All calculations were carried by Gaussian 16,<sup>S7</sup> using the global hybrid MN15 functional by Truhlar and coworkers<sup>S8</sup> in combination with the def2-TZVP basis set by Ahlrichs and coworkers.<sup>S9-S10</sup> Relativistic effective core potentials of 28, 46 and 60 electrons were used to describe the core electrons of Ag, Sb and Au, respectively.<sup>S11-S12</sup> The MN15 method was selected based on its especially good performance for noncovalent interactions and excitation energies.<sup>S8</sup>

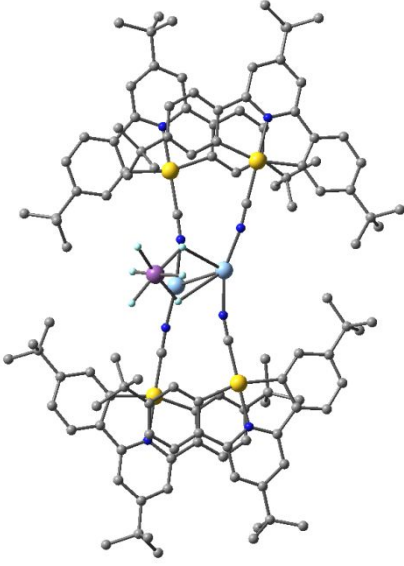
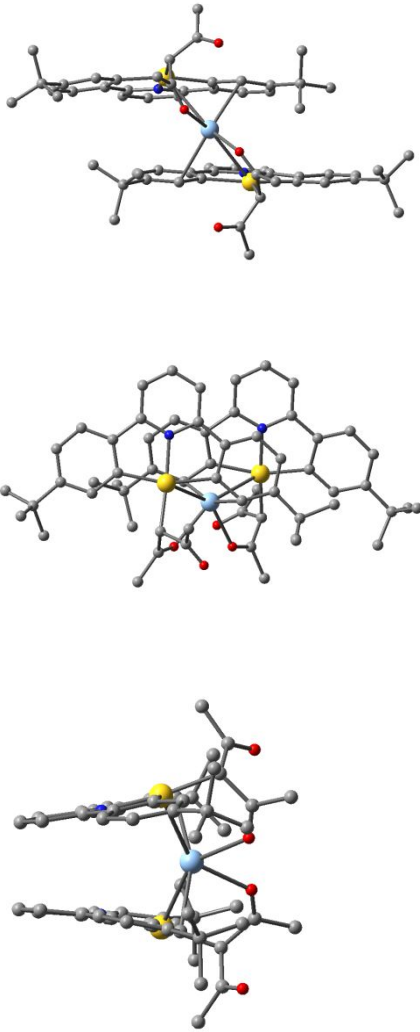
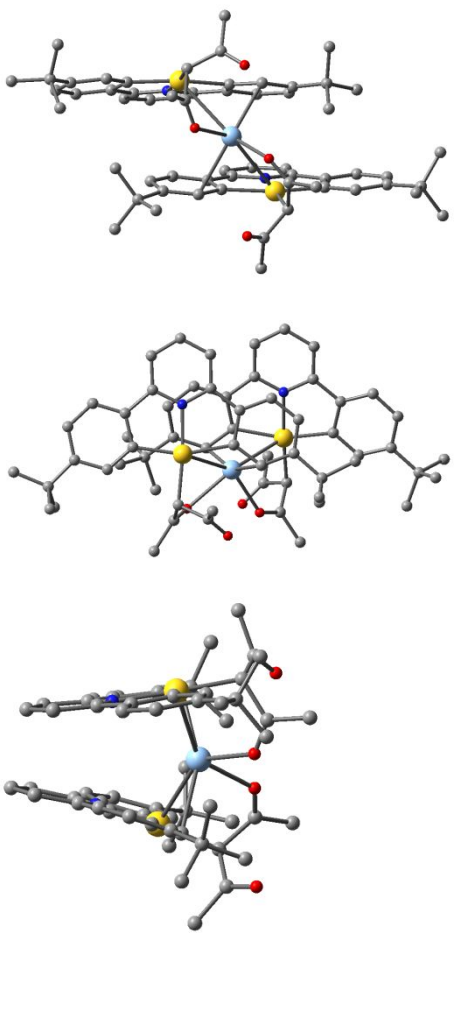
**Table S4.1.** Optimized structures of the complexes

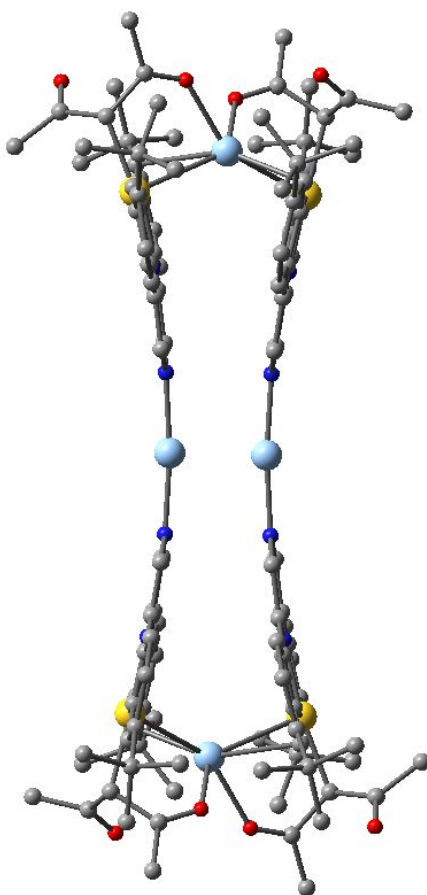
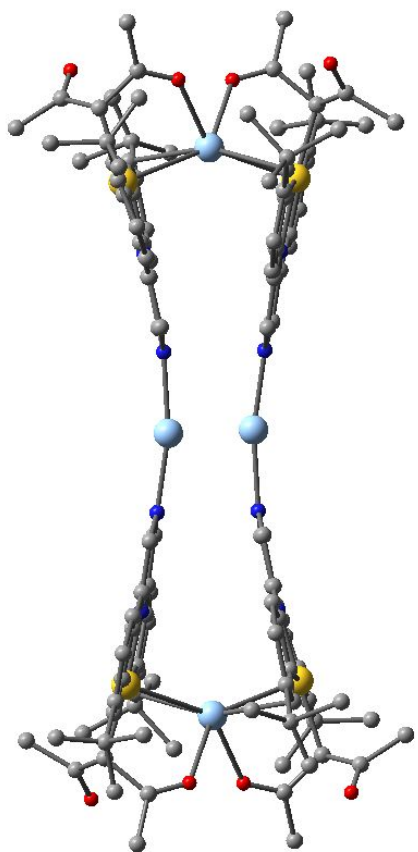
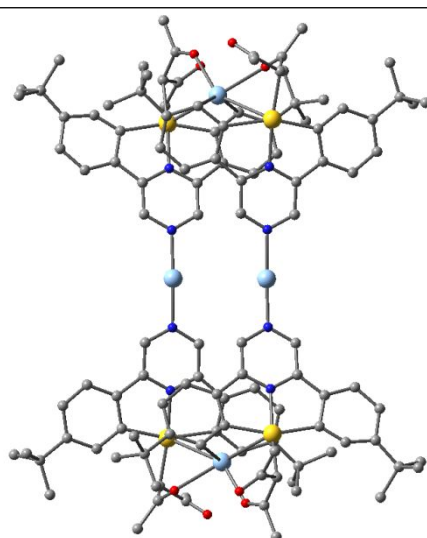
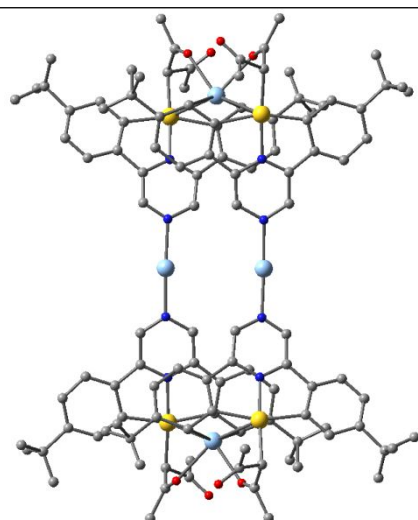
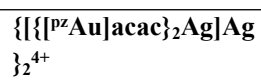
| Structures   | Crystal structure   | Optimized structure  |
|--------------|---|--|
| [pzAu]CN     |   |   |
| [tBu-pyAu]CN |   |  |
| [pzAu]acac   |  |  |

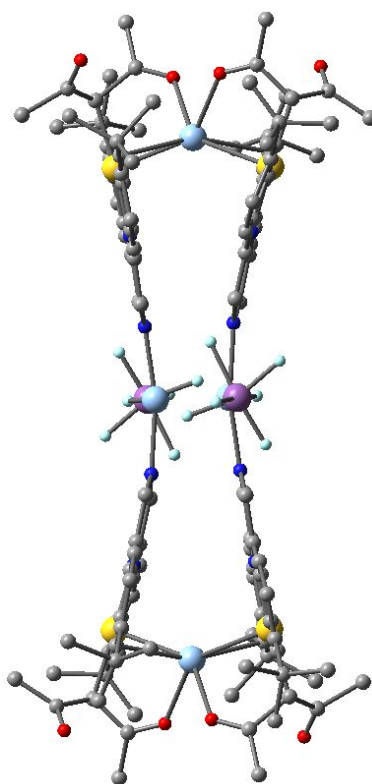
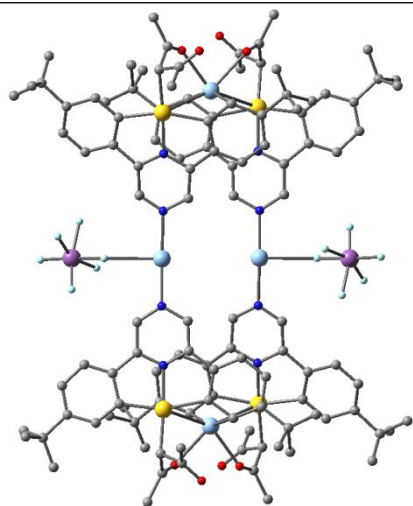
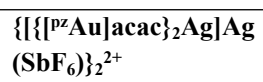


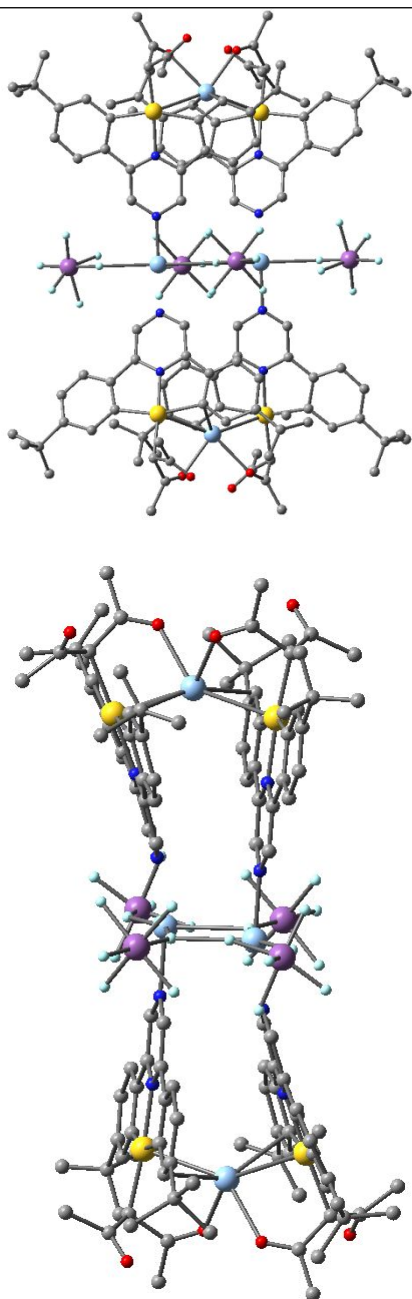
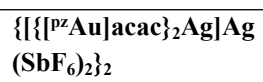
|  |   |  |
|--|---|--|
| $[\text{pyAu}]\text{acac}$                   |   |    |
| $\{[\text{pzAu}]\text{CN}\}_2\text{Ag}^+$    |   |   |
| $\{[\text{tBupyAu}]\text{CN}\}_2\text{Ag}^+$ |  |  |

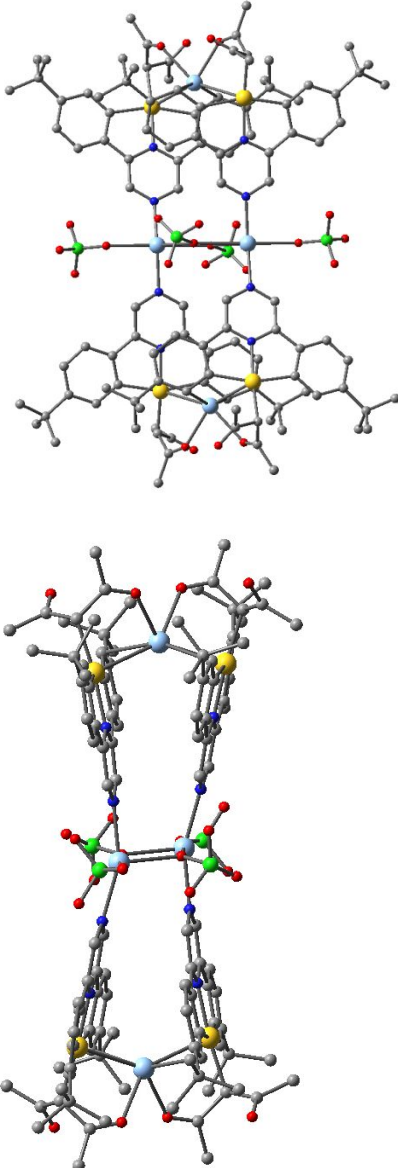


|   |  |   |
|---|--|---|
| <p><math>[[\{\text{tBupyAu}\}\text{CN}\}_2\text{Ag}]_2</math><br/><math>(\text{SbF}_6)^+</math></p> |   |   |
| <p><math>[[\{\text{pyAu}\}\text{acac}\}_2\text{Ag}]^+</math></p>                                    |  |  |

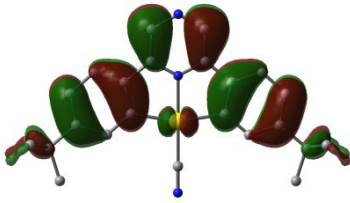


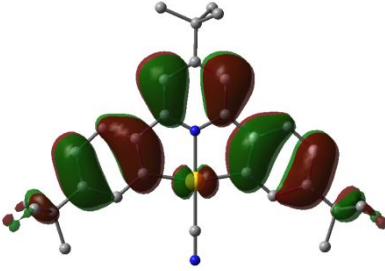
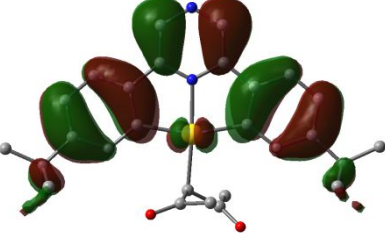
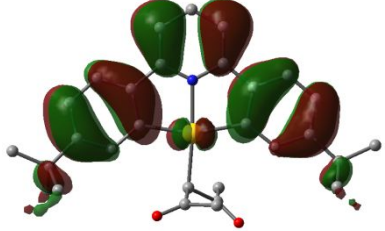
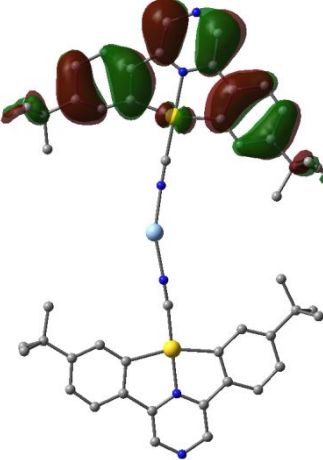
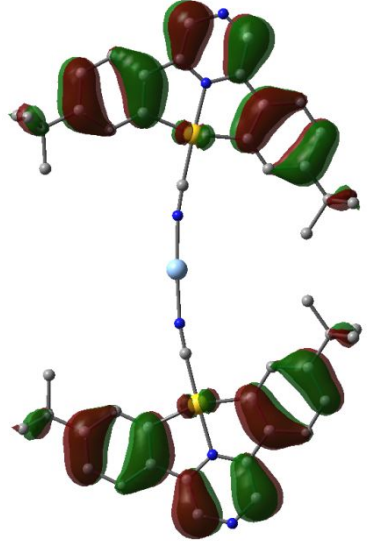




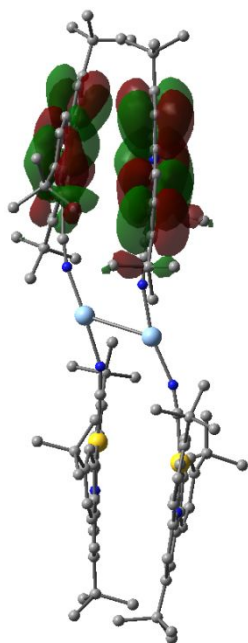
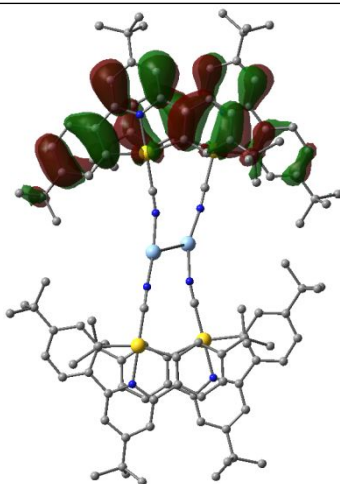
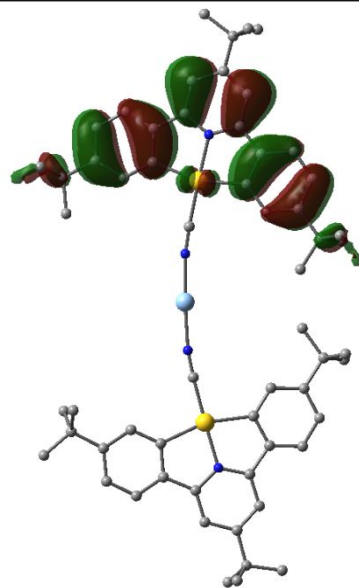
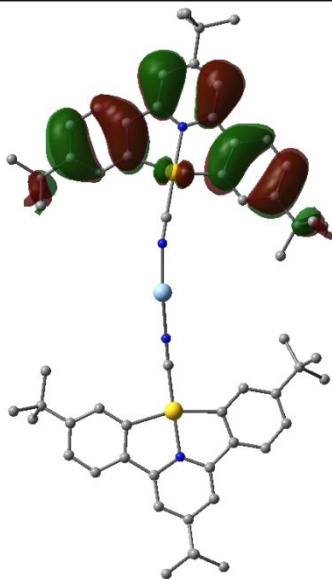
|  |  |  |
|--|--|--|
| $\{ \{ [^{197}\text{Au}] \text{acac} \}_2 \text{Ag} \}_2 (\text{ClO}_4)_2$ |  |  |
|--|--|--|

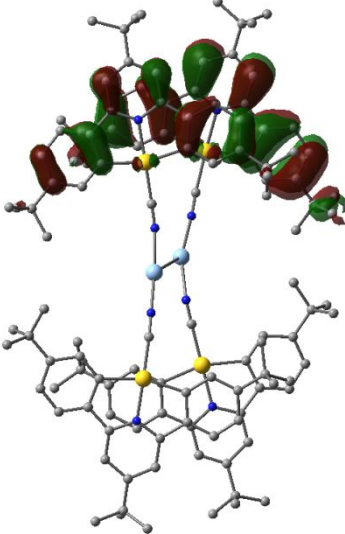
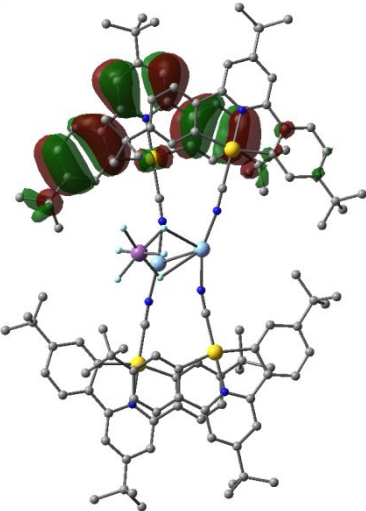
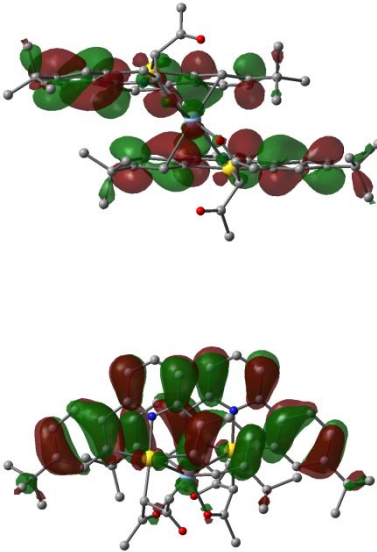
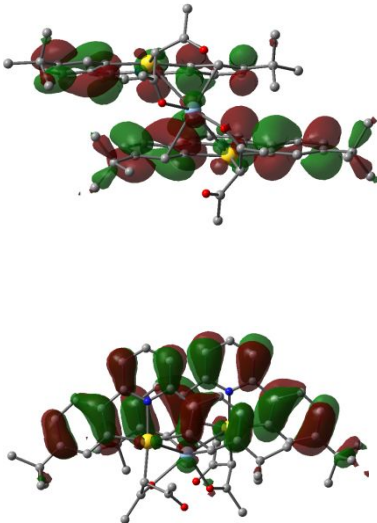
**Table S4.2.** HOMO orbitals of the complexes

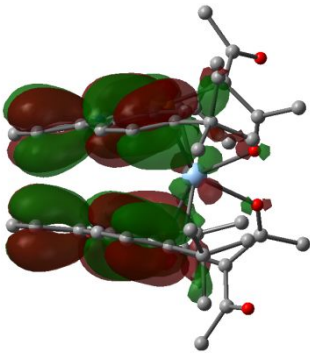
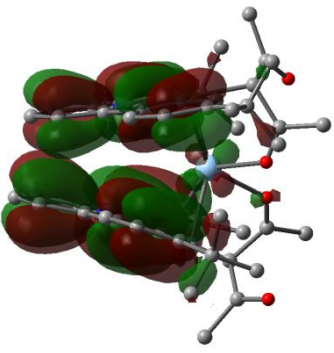
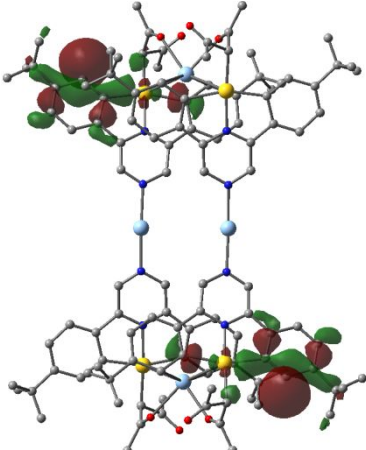
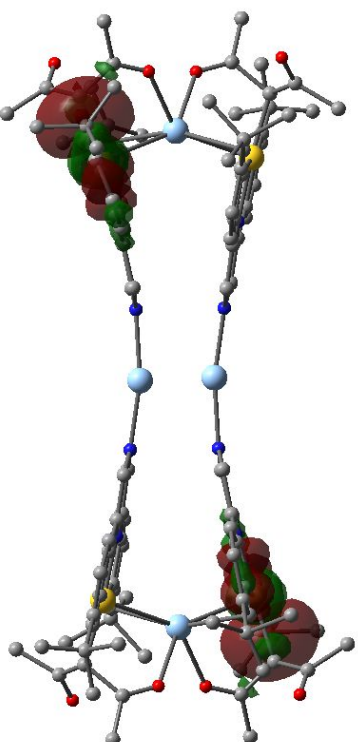
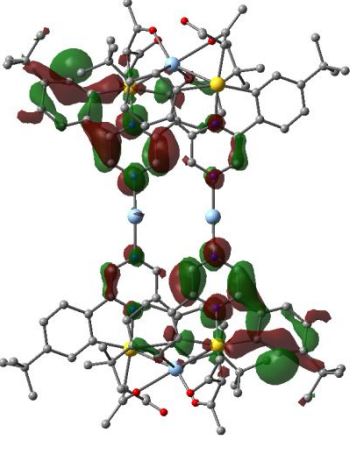
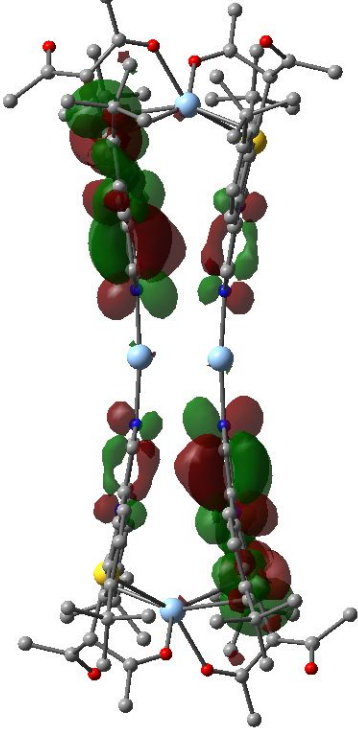
| HOMO                         | Crystal structure | Optimized structure   |
|------------------------------|-------------------|---|
| $[^{197}\text{Au}]\text{CN}$ |                   |  |

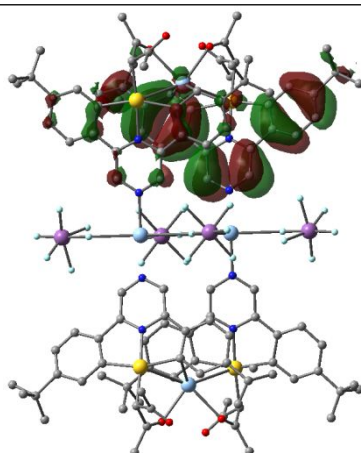
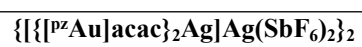
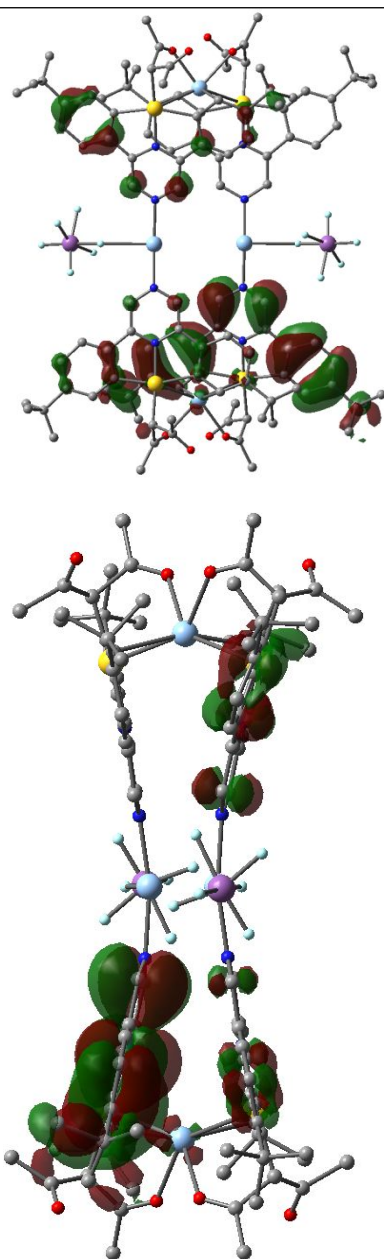
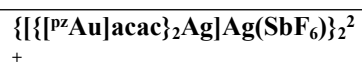
|   |   |   |
|---|---|---|
| $[\text{tBu-pyAu}]\text{CN}$              |   |    |
| $[\text{pzAu}]\text{acac}$                |   |    |
| $[\text{pyAu}]\text{acac}$                |   |   |
| $\{[\text{pzAu}]\text{CN}\}_2\text{Ag}^+$ |  |  |

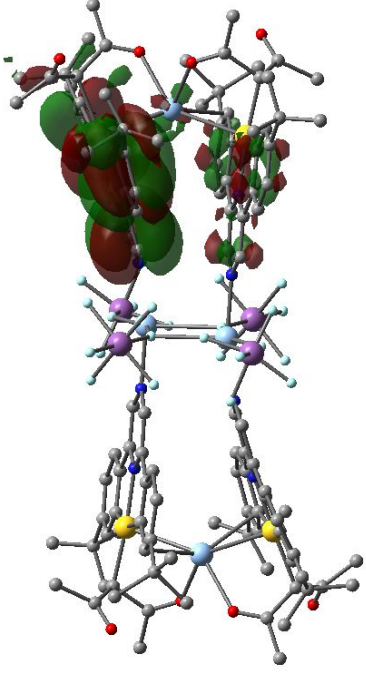
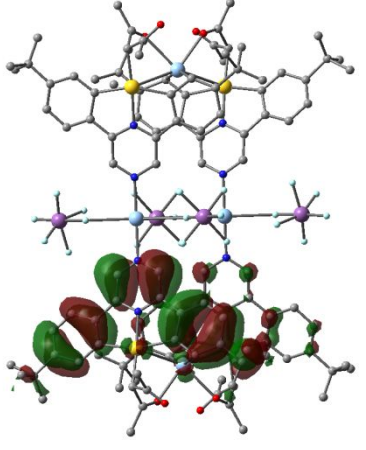
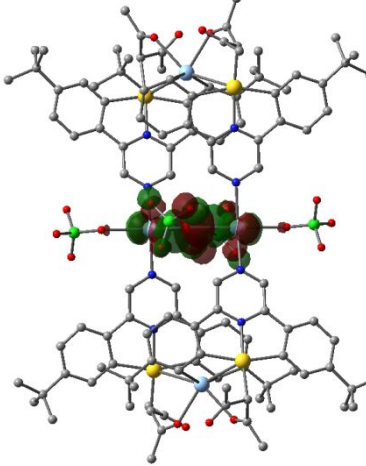


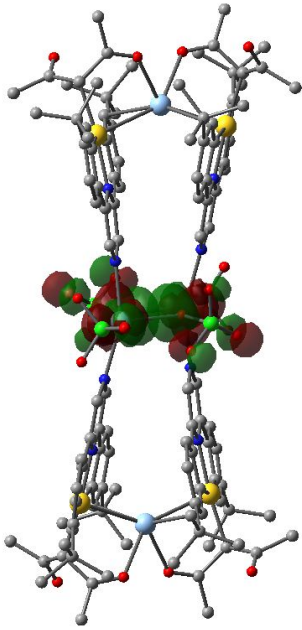
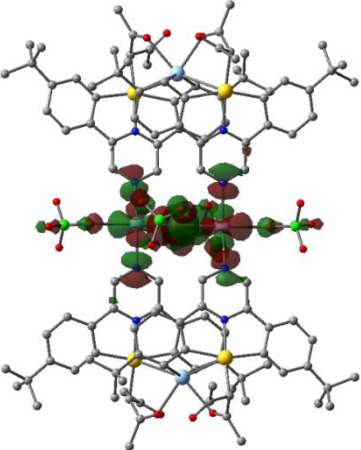


|  |   |   |
|--|---|---|
| $[[\{t\text{BupyAu}\}\text{CN}\}_2\text{Ag}]_2^{2+}$<br><br>HOMO-1 |    |   |
| $[[\{t\text{BupyAu}\}\text{CN}\}_2\text{Ag}]_2(\text{SbF}_6)^+$    |   |   |
| $[[\{p\text{yAu}\}\text{acac}\}_2\text{Ag}]^+$                     |  |  |

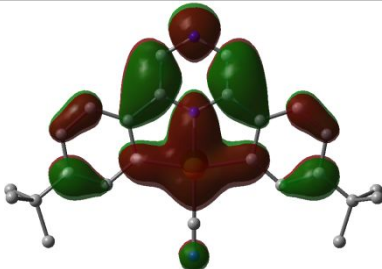
|   |   |   |
|---|---|---|
|   |    |    |
| $\{[\text{PzAu}]\text{acac}\}_2\text{Ag}[\text{Ag}]_2^{4+}$ | <br> | <br> |



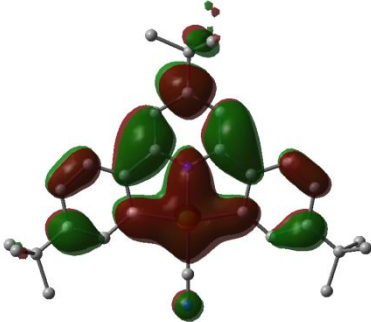
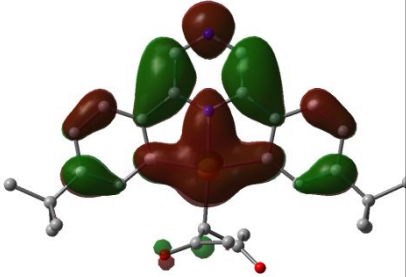
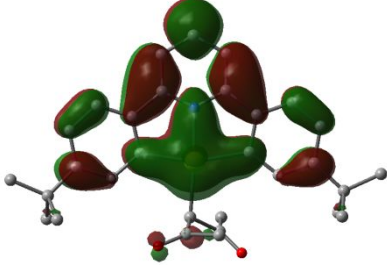
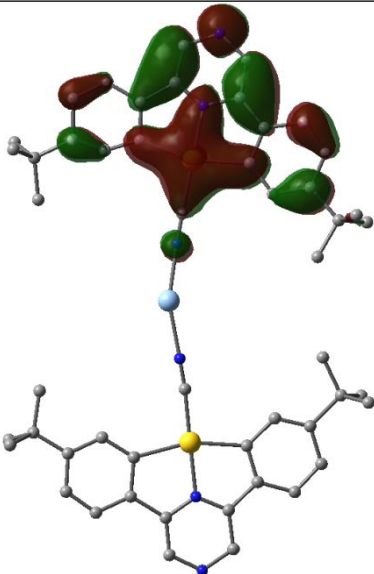
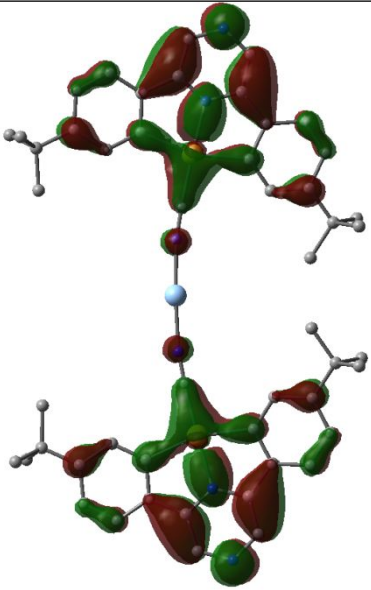
|   |   |  |
|---|---|--|
|   |    |  |
| $\{[\text{pzaAu}(\text{acac})_2\text{Ag}][\text{Ag}(\text{SbF}_6)_2]\}_2$<br>HOMO-1 |   |  |
| $\{[\text{pzaAu}(\text{acac})_2\text{Ag}][\text{Ag}(\text{ClO}_4)_2]\}_2$           |  |  |

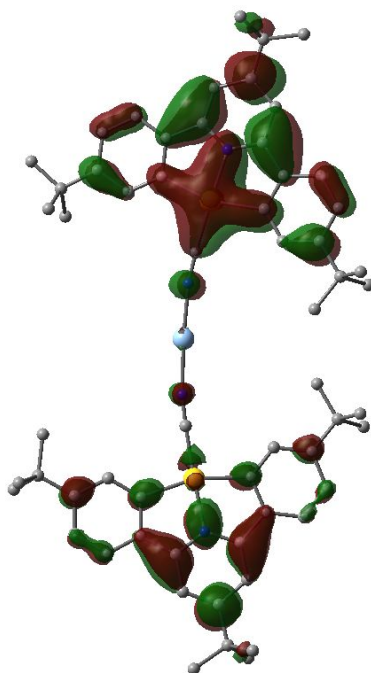
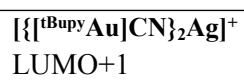
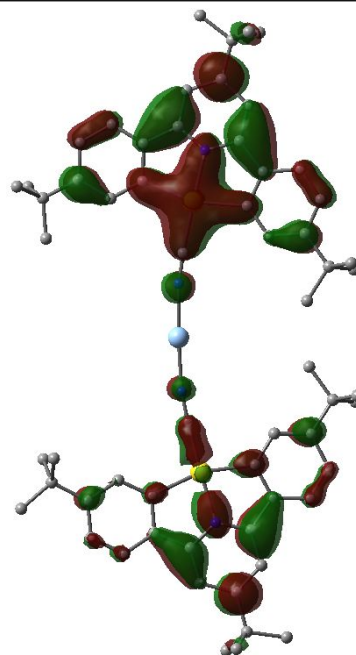
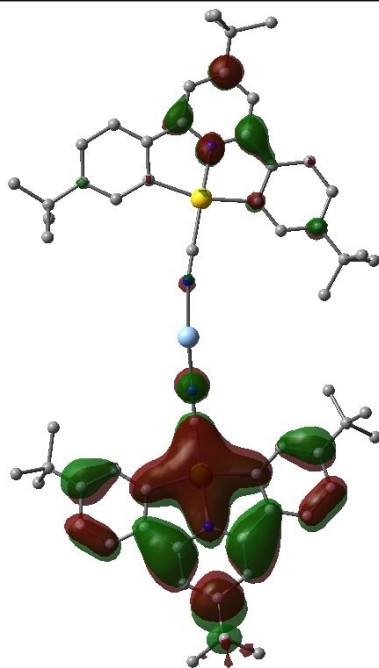
|  |  |  |
|--|--|--|
|  |   |  |
| $\{[p^zAu]acac\}_2Ag[Ag(ClO_4)_2]_2$<br>HOMO-1 |  |  |

**Table S4.3.** LUMO orbitals of the complexes

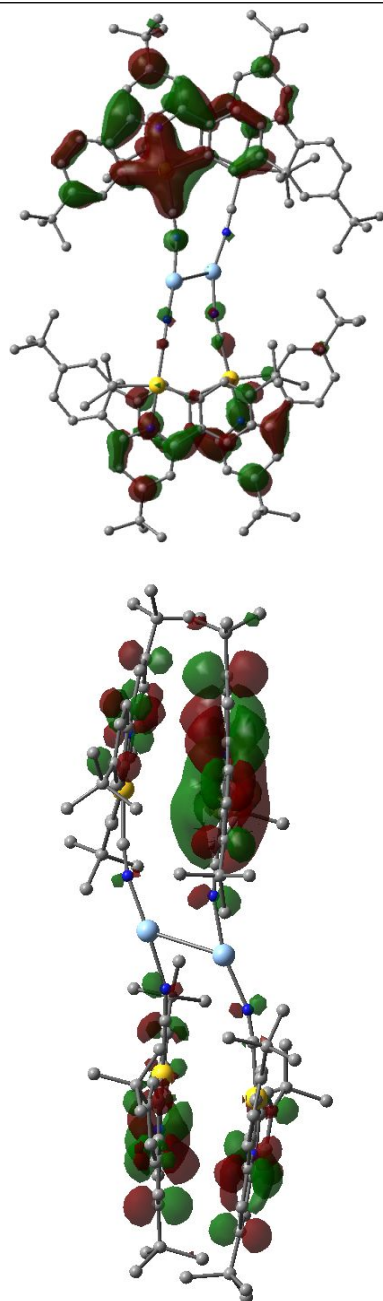
| LUMO        | Crystal structure | Optimized structure   |
|-------------|-------------------|---|
| $[p^zAu]CN$ |                   |  |



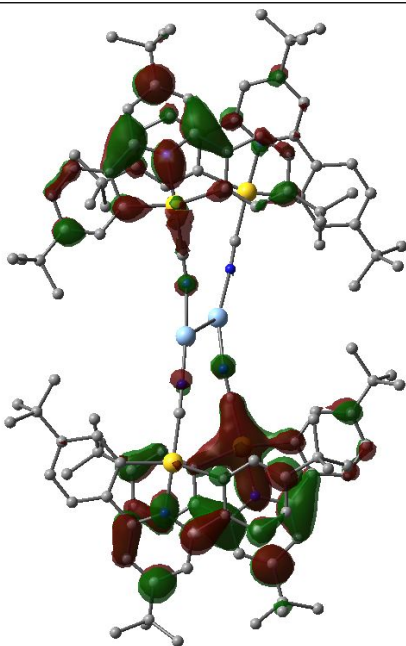
|   |   |   |
|---|---|---|
| $[\text{tBu-pyAu}]\text{CN}$              |   |    |
| $[\text{pzAu}]\text{acac}$                |   |    |
| $[\text{pyAu}]\text{acac}$                |   |   |
| $\{[\text{pzAu}]\text{CN}\}_2\text{Ag}^+$ |  |  |



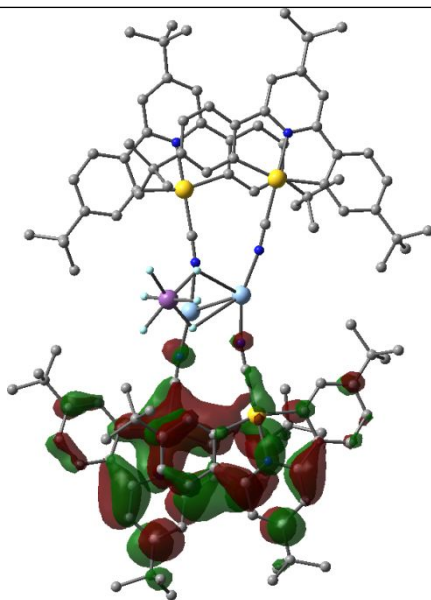




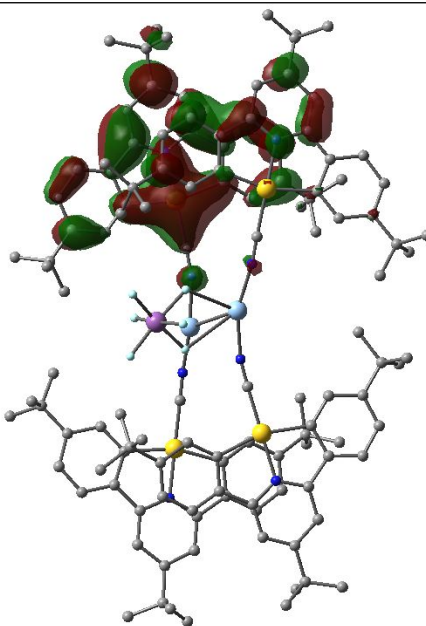
$[[\{t\text{BupyAu}\}\text{CN}\}_2\text{Ag}]_2^{2+}$   
LUMO+1



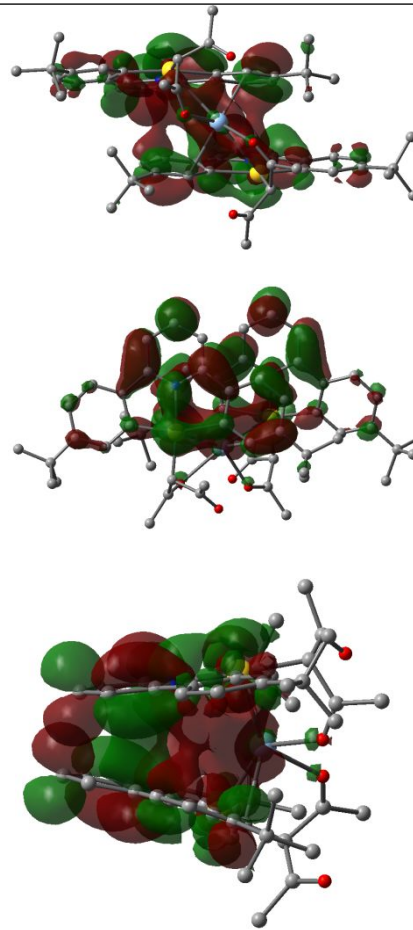
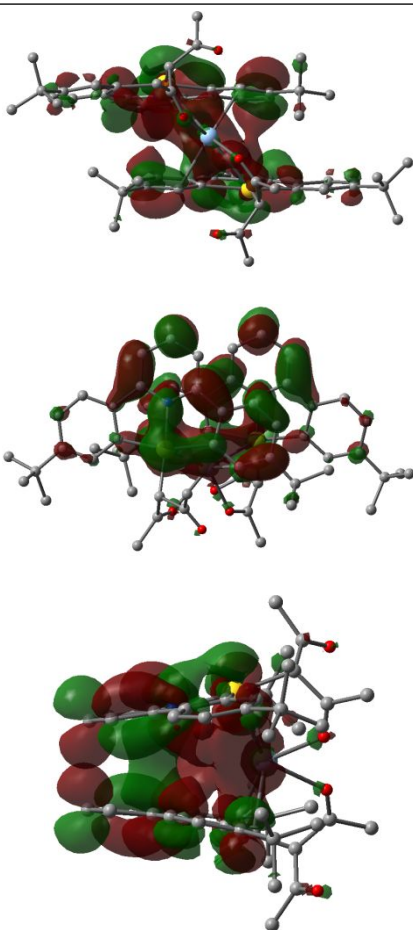
$[[\{t\text{BupyAu}\}\text{CN}\}_2\text{Ag}]_2(\text{SbF}_6)^+$

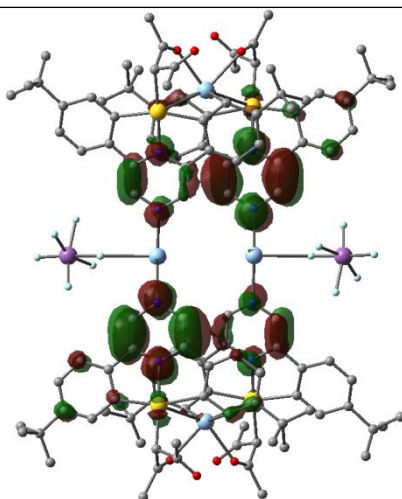
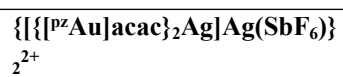
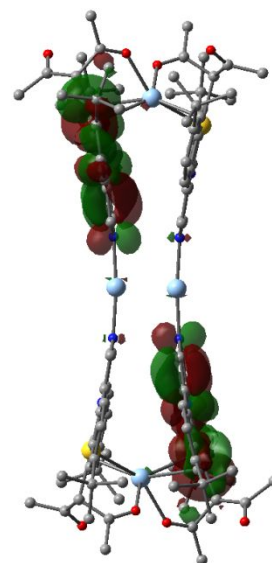
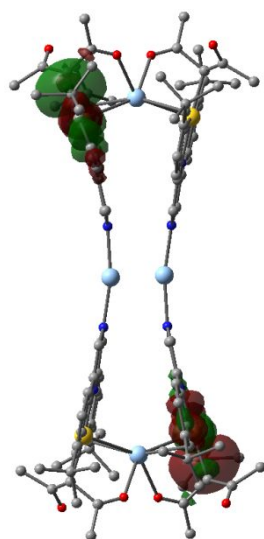
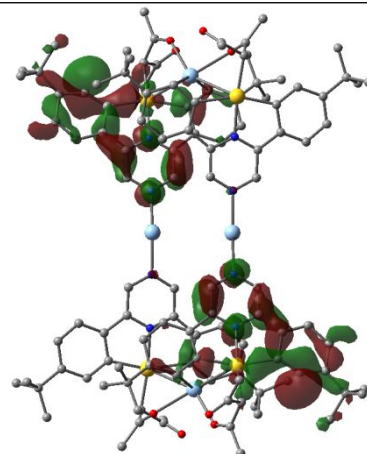
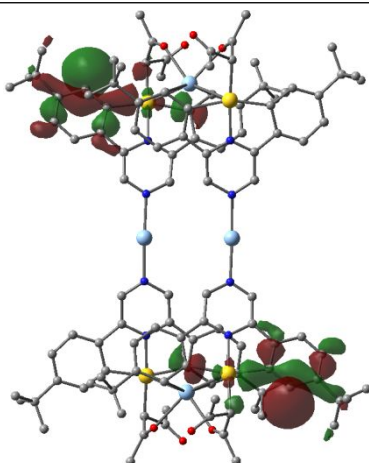
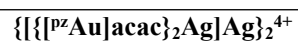


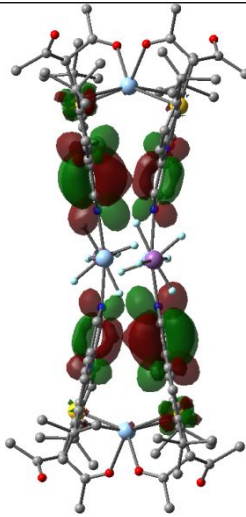
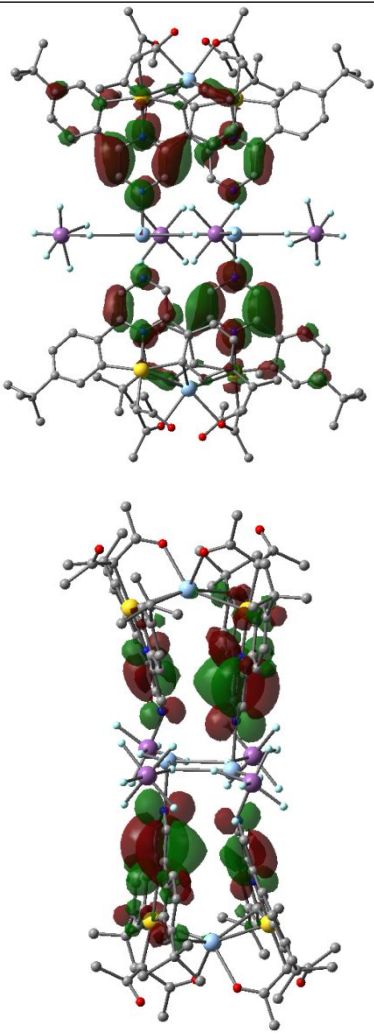
$[[\{[{}^{\text{tBup}}\text{Au}]\text{CN}\}_2\text{Ag}]_2(\text{SbF}_6)]^+$   
LUMO+1

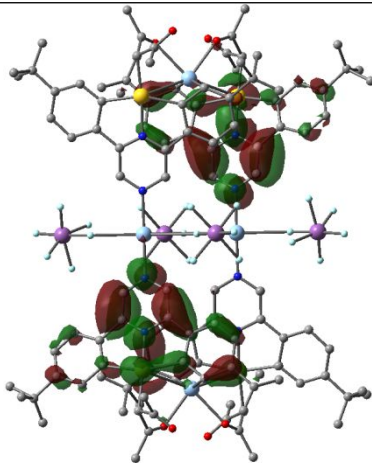
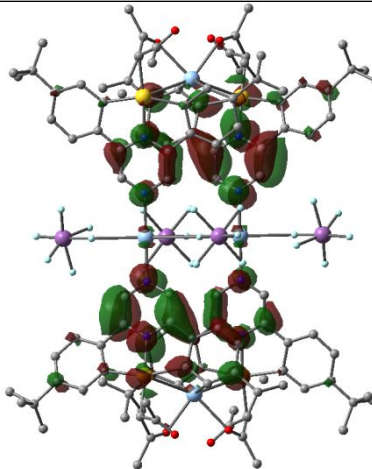
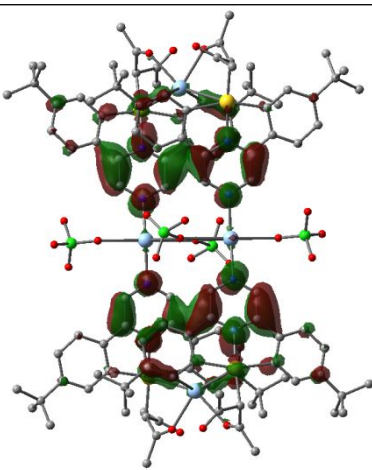


$[[\{[{}^{\text{py}}\text{Au}]\text{acac}\}_2\text{Ag}]^+$





|  |  |  |
|--|--|--|
|  |   |  |
| $\{ \{ [P^zAu]acac \}_2 Ag [Ag(SbF_6)_2] \}_2$ |  |  |

|  |   |  |
|--|---|--|
| $\{ \{ [^{197}\text{Au}] \text{acac} \}_2 \text{Ag} [ \text{Ag} (\text{SbF}_6)_2 ] \}_2$<br>LUMO+2 |    |  |
| $\{ \{ [^{197}\text{Au}] \text{acac} \}_2 \text{Ag} [ \text{Ag} (\text{SbF}_6)_2 ] \}_2$<br>LUMO+3 |   |  |
| $\{ \{ [^{197}\text{Au}] \text{acac} \}_2 \text{Ag} [ \text{Ag} (\text{ClO}_4)_2 ] \}_2$           |  |  |

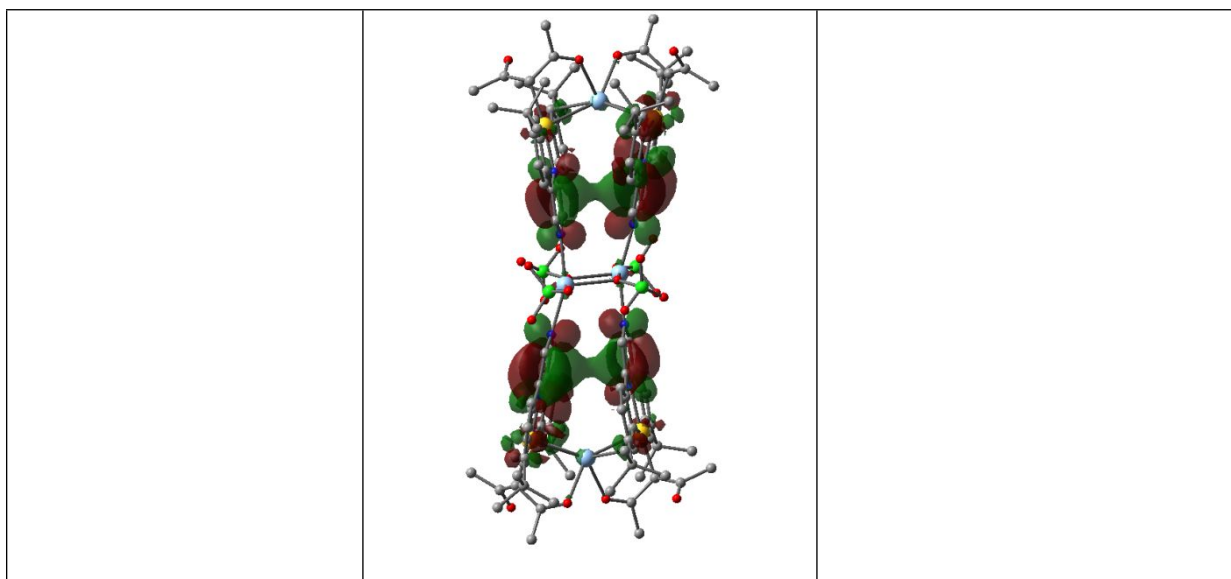


**Table S4.4.** Calculated electronic transitions of the complexes.

| Energies / eV  | Crystal structure               |  |   | Optimized structure |
|--|---------------------------------|--|---|---------------------|
|  | LUMO-HOMO (scaled) <sup>a</sup> | S1@S0 (osc. strength)                          | S0-S1 character   | LUMO-HOMO (scaled)  |
| [ <sup>pz</sup> Au]CN  |                                 | 3.12 (0.067) <sup>b</sup>                      | HOMO → LUMO (94%)   | 4.91 (3.44)         |
| [ <sup>tBu-py</sup> Au]CN  |                                 | 3.35 (0.085) <sup>b</sup>                      | HOMO → LUMO (94%)   | 5.19 (3.73)         |
| [ <sup>pz</sup> Au]acac  | 4.98 (3.52)                     | crystal 3.17 (0.098)<br>optimized 3.19 (0.099) | HOMO → LUMO (94%)   | 5.01 (3.55)         |
| [ <sup>py</sup> Au]acac  |                                 | 3.39 (0.088) <sup>b</sup>                      | HOMO → LUMO (93%)   | 5.23 (3.77)         |
| {[ <sup>pz</sup> Au]CN} <sub>2</sub> Ag] <sup>+</sup>                                      | 4.68 (3.22)                     | 2.88 (0.091)                                   | HOMO → LUMO (95%)   | 4.77 (3.31)         |
| {[ <sup>tBupy</sup> Au]CN} <sub>2</sub> Ag] <sup>+</sup>                                   | 5.02 (3.56)                     | 3.24 (0.060)                                   | HOMO → LUMO+1 (80%)   | 5.06 (3.59)         |
| {[ <sup>tBupy</sup> Au]CN} <sub>2</sub> Ag] <sub>2</sub> <sup>2+</sup>                     | 4.90 (3.44)                     | 3.16 (0.034)                                   | HOMO → LUMO (42%)<br><br>HOMO → LUMO+1 (26%)<br><br>HOMO-1 → LUMO (11%) |                     |
| {[ <sup>tBupy</sup> Au]CN} <sub>2</sub> Ag] <sub>2</sub> (SbF <sub>6</sub> ) <sup>+</sup>  | 4.82 (3.35)                     | 3.20 (0.037)                                   | HOMO → LUMO+1 (78%)   |                     |
| {[ <sup>py</sup> Au]acac} <sub>2</sub> Ag] <sup>+</sup>                                    | 4.83 (3.37)                     | 3.19 (0.110)                                   | HOMO → LUMO (77%)   | 4.88 (3.42)         |
| {[ <sup>pz</sup> Au]acac} <sub>2</sub> Ag]Ag] <sub>2</sub> <sup>4+</sup>                   | 0.35                            | 0.06 (0.007)                                   |   | 0.61                |
| {[ <sup>pz</sup> Au]acac} <sub>2</sub> Ag]Ag(SbF <sub>6</sub> ) <sub>2</sub> <sup>2+</sup> | 3.99 (2.53)                     |  |   |                     |
| {[ <sup>pz</sup> Au]acac} <sub>2</sub> Ag]Ag(SbF <sub>6</sub> ) <sub>2</sub>               | 4.29 (2.82)                     | 2.79 (0.000) <sup>c</sup>                      | HOMO →  |                     |



|   |             |               |  |  |
|---|-------------|---------------|--|--|
|   |             |               | LUMO+2 (20%)<br><br>HOMO-1 →<br>LUMO+2 (17%)<br><br>HOMO-1 →<br>LUMO (15%)<br><br>HOMO →<br>LUMO (12%)<br><br>HOMO-1 →<br>LUMO+3 (11%)<br><br>HOMO-1 →<br>LUMO+3 (11%) |  |
| <b>{{[P<sup>z</sup>Au]acac}<sub>2</sub>Ag[Ag(CIO<sub>4</sub>)<sub>2</sub>]<sub>2</sub>}</b> | 3.45 (1.99) | 2.15 (0.0045) | HOMO-1 →<br>LUMO (81%)   |  |

<sup>a</sup>scaled by using CMA1 as a reference: calculated = 4.28eV, exp = 2.82eV, Δ = 1.46eV. <sup>b</sup>For optimized structure (since there was no crystal structure for this complex). S2@S0 = 2.80eV with very similar orbital contributions but with oscillator strength of 0.2386.

## S.5 Diffusion NMR

<sup>1</sup>H PGSE NMR measurements were performed by using a double stimulated echo sequence with longitudinal eddy current delay on a Bruker DRX 300 spectrometer equipped with a smartprobe and Z-gradient coil, at 297K without spinning. In the typical PGSE experiment, the dependence of the resonance intensity (*I*) on a constant waiting time and on a varied gradient strength *G* is described by the following equation:

$$\ln \frac{I}{I_0} = (\gamma \delta^2) D_t \left( \delta - \frac{\Delta}{3} \right) G^2$$

where *I* is the intensity of the observed spin echo, *I*<sub>0</sub> the intensity of the spin echo in the absence of gradient, *D*<sub>t</sub> the self-diffusion coefficient, Δ the delay between the midpoints of the gradients, δ the length of the gradient pulse, and γ the magnetogyric ratio. The shape of the gradients was rectangular, their length δ was 4–5 ms, and their strength *G* was varied during the experiments. All spectra were acquired for 64K points and a spectral width of 6200 Hz and processed with a line broadening of 1.0. The semi-logarithmic plots of ln(*I*/*I*<sub>0</sub>) versus *G*<sup>2</sup> were fitted by using a standard linear regression algorithm. Different values of *G* and number of transients were used for different samples.

The self-diffusion coefficient *D*<sub>t</sub>, which is directly proportional to the slope of the regression line obtained by plotting ln(*I*/*I*<sub>0</sub>) versus *G*<sup>2</sup>, was estimated by evaluating the proportionality constant for a sample of HDO (5%) in D<sub>2</sub>O (known diffusion coefficients in the range 274–318 K)<sup>S13</sup> under the exact same conditions as the sample of interest. The solvent was taken as internal standard. The actual concentration of the samples was measured by relative integration to an external standard.

The relationship between *D*<sub>t</sub> and hydrodynamic dimensions is expressed by the modified Stokes-Einstein equation:

$$D_t = \frac{kT}{\pi \eta f c^3 \sqrt{abd}}$$

where *k* is the Boltzmann constant, *T* is the temperature, η is the solution viscosity, *c* is the “size factor”, which depends on the solute-solvent radius ratio and *f* is the “shape factor”, which takes into account the deviation from sphericity of the diffusing molecule. *a*, *b* and *d* are the semi-axes of the ellipsoid that better approximates the shape of the diffusing molecule.<sup>S14</sup>

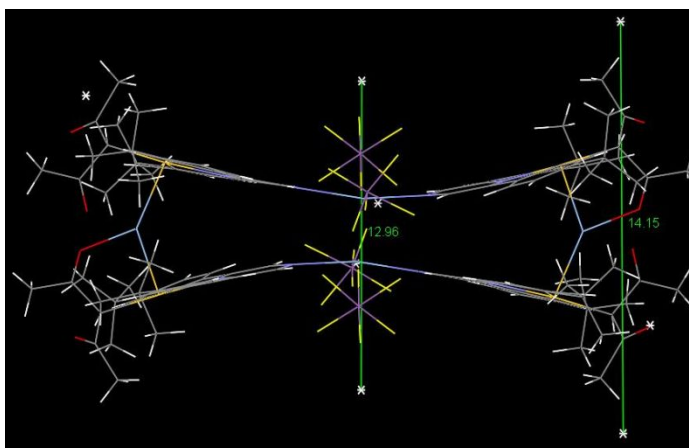
Structural parameter values (*P* = *f c*<sup>3</sup>√*abd* = *kT* / πη*D*<sub>t</sub>) were derived from the measured *D*<sub>t</sub> values at different concentration in CD<sub>2</sub>Cl<sub>2</sub> and reported in Table S5.1

Theoretical *P* values for **3ClO<sub>4</sub>** and **3SbF<sub>6</sub>** were obtained from the crystal structures of the two compounds, by approximating their Van der Waals volume to that of an oblate ellipsoid (*a*<*b*=*d*), as showed below for **3SbF<sub>6</sub>**.

**Table S.5.1** Self-diffusion coefficients ( $D_t$ ) and structural parameters ( $P$ ) obtained for  $[\text{p}^z\text{Au}]\text{acac}$ ,  $3\text{SbF}_6$  and  $3\text{ClO}_4$  in  $\text{CD}_2\text{Cl}_2$  at room temperature at different concentration values ( $c$ ).

| $c$ (mM)   | $10^{-10} D_t$ ( $\text{m}^2 \text{s}^{-1}$ ) | $P$ (Å)        |
|--|---|----------------|
| <b><math>[\text{p}^z\text{Au}]\text{acac}</math> (<math>P=29.0</math>)</b> |   |                |
| 0.7  | $10.1 \pm 0.3$                                | $30.4 \pm 1.5$ |
| 3.0  | $10.1 \pm 0.3$                                | $30.4 \pm 1.5$ |
| 24.0   | $10.0 \pm 0.3$                                | $30.5 \pm 1.5$ |
| <b><math>3\text{SbF}_6</math> (<math>P=57.7</math>)</b>                    |   |                |
| 0.8  | $0.51 \pm 0.02$                               | $59.8 \pm 3.0$ |
| 2.7  | $0.51 \pm 0.02$                               | $59.9 \pm 3.0$ |
| 6.0  | $0.51 \pm 0.02$                               | $59.6 \pm 3.0$ |
| <b><math>3\text{ClO}_4</math> (<math>P=57.7</math>)</b>                    |   |                |
| 0.5  | $0.53 \pm 0.02$                               | $57.7 \pm 2.9$ |
| 1.8  | $0.52 \pm 0.02$                               | $58.6 \pm 2.9$ |
| 5.3  | $0.51 \pm 0.02$                               | $59.9 \pm 3.0$ |

Semixis calculations for **3SbF<sub>6</sub>** (approximation to oblate ellipsoid)



**Revolution axis**

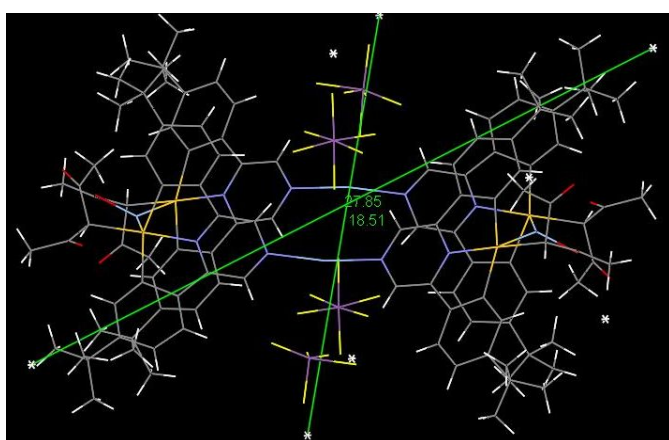
$$(12.96 \text{ \AA} + 14.15 \text{ \AA})/2 = 13.555 \text{ \AA}$$

$$\text{Semiaxis } a = 6.7775 \text{ \AA}$$

**Rotation axis**

$$(27.85 \text{ \AA} + 18.51 \text{ \AA})/2 = 23.18 \text{ \AA}$$

$$\text{Semiaxis } b = 11.59 \text{ \AA}$$



$$f_{\text{oblate}} = \frac{\sqrt{\left(\frac{b}{a}\right)^2 - 1}}{\left(\frac{b}{a}\right)^{\frac{2}{3}} \arctan \sqrt{\left(\frac{b}{a}\right)^2 - 1}} = 1.025$$

$$P_{\text{oblate}} = f \frac{6}{1 + \left(0.695 \cdot \frac{r_{CD2Cl2}}{\sqrt[3]{ab^2}}\right)^{2.234}} \sqrt[3]{ab^2} = 57.7 \text{ \AA}$$

## S5. References

- S1 *Programs CrysAlisPro*, Oxford Diffraction Ltd., Abingdon, UK (2010)
- S2 Sheldrick, G. M. *Acta Cryst.* **2008**, *A64*, 112.
- S3 Spek, A. L. (2006) PLATON – A Multipurpose Crystallographic Tool, Utrecht University, Utrecht, The Netherlands. A. L. Spek, *Acta Cryst.* **1990**, *A46*, C34
- S4 Farrugia, L. J. *J. Appl. Crystallogr.* **1999**, *32*, 837.
- S5 ‘*International Tables for X-ray Crystallography*’, Kluwer Academic Publishers, Dordrecht. Vol. C. **1992**, pp. 500, 219 and 193.
- S6 F. Furche, D. Rappoport, Density functional methods for excited states: equilibrium structure and electronic spectra. In *Computational Photochemistry*; M. Olivucci, Ed.; Elsevier: Amsterdam, 2005; pp. 93–128.
- S7 Gaussian 16, Revision A.03, M.J. Frisch, G.W. Trucks, H.B. Schlegel, G.E. Scuseria, M.A. Robb, J.R. Cheeseman, G. Scalmani, V. Barone, G.A. Petersson, H. Nakatsuji, X. Li, M. Caricato, A.V. Marenich, J. Bloino, B.G. Janesko, R. Gomperts, B. Mennucci, H.P. Hratchian, J.V. Ortiz, A.F. Izmaylov, J.L. Sonnenberg, D. Williams-Young, F. Ding, F. Lipparini, F. Egidi, J. Goings, B. Peng, A. Petrone, T. Henderson, D. Ranasinghe, V.G. Zakrzewski, J. Gao, N. Rega, G. Zheng, W. Liang, M. Hada, M. Ehara, K. Toyota, R. Fukuda, J. Hasegawa, M. Ishida, T. Nakajima, Y. Honda, O. Kitao, H. Nakai, T. Vreven, K. Throssell, J.A. Montgomery, Jr., J.E. Peralta, F. Ogliaro, M.J. Bearpark, J.J. Heyd, E.N. Brothers, K.N. Kudin, V.N. Staroverov, T.A. Keith, R. Kobayashi, J. Normand, K. Raghavachari, A.P. Rendell, J.C. Burant, S.S. Iyengar, J. Tomasi, M. Cossi, J.M. Millam, M. Klene, C. Adamo, R. Cammi, J.W. Ochterski, R.L. Martin, K. Morokuma, O. Farkas, J.B. Foresman, D.J. Fox, Gaussian, Inc., Wallingford CT, **2016**.
- S8 H.S. Yu, X. He, S.L. Li, D.G. Truhlar, *Chem. Sci.* **2016**, *7*, 5032–5051.
- S9 F., Weigend, M. Häser, H. Patzelt, R. Ahlrichs, *Chem. Phys. Lett.* **1998**, *294*, 143–152.
- S10 F. Weigend, R. Ahlrichs, *Phys. Chem. Chem. Phys.* **2005**, *7*, 3297–3305.
- S11 D. Andrae, U. Haeussermann, M. Dolg, H. Stoll, H. Preuss, *Theor. Chim. Acta* **1990**, *77*, 123–141.
- S12 B. Metz, H. Stoll, M. Dolg, *J. Chem. Phys.* **2000**, *113*, 2563–2569.

S13 (a) Tyrrell, H. J. W.; Harris, K. R. *Diffusion in Liquids*; Butterworth: London, 1984. (b) Mills, R. *J. Phys. Chem.* **1973**, *77*, 685.

S14 (a) Macchioni, A.; Ciancaleoni, G.; Zuccaccia, C.; Zuccaccia, D. *Chem. Soc. Rev.* **2008**, *37*, 479. (b) Zuccaccia, D.; Macchioni, A. *Organometallics* **2005**, *24*, 3476.